ITER fast ion collective Thomson scattering. Conceptual design of 60 GHz system

Meo, Fernando; Bindslev, Henrik; Korsholm, Søren Bang

Publication date:
2007

Document Version
Publisher's PDF, also known as Version of record

Risø-R-Report

ITER fast ion collective Thomson scattering

Conceptual design of 60 GHz system

Fernando Meo, Henrik Bindslev and Søren B. Korsholm

Risø-R-1600(EN)

Risø National Laboratory
Technical University of Denmark
Roskilde, Denmark
August 2007

Authors: Fernando Meo, Henrik Bindslev and Søren B. Korsholm
Title: ITER fast ion collective Thomson scattering, conceptual design of 60 GHz system.
Department: Optics and Plasma Research Department.

Risø-R-1600(EN)
August 2007

Abstract (max. 2000 char.):

The physics feasibility study [H. Bindslev, F. Meo, S. Korsholm, ITER Report, "ITER Fast Ion Collective Thomson Scattering, Feasibility study", contract number EFDA 01.654,]http://sitecoremedia.risoe.dk/research/Fusion_CTS/Documents/CTS_Feasibility.pdf

The collective Thomson scattering diagnostic for ITER at the 60 GHz range is capable of measuring the fast ion distribution parallel and perpendicular to the magnetic field at different radial locations simultaneously. The design is robust technologically with no moveable components near the plasma. The fast ion CTS diagnostic consists of two separate systems. Each system has its own RF launcher and separate set of detectors. The first system measures the perpendicular component of the fast ion velocity distribution. It consists of radially directed RF launcher and receiver, both located in the equatorial port on the low field side (LFS). This system will be referred to by the acronym *LFS-BS* system referring to the location of the receiver and the fact that it measures backscattered radiation. The second part of the CTS diagnostic measures the parallel component of the fast ion distribution. It consists of an RF launcher located in the mid-plane port on the LFS and a receiver mounted on the inner vacuum vessel wall that views the plasma from between two blanket modules. This system will be referred to as *HFS-FS* referring to the location of the receivers and that they measure forward scattered radiation. The design of both LFS-BS and HFS-FS receivers is aimed at measuring at different spatial locations simultaneously with no moveable components near the plasma. This report is a preliminary study of the hardware design and engineering constraints for this frequency range. Section 2 conceptually describes the two systems and their main components. Section 3 clarifies the impact of design parameters such as beam widths and scattering angle on the CTS measurements. With this in hand, the ITER measurement requirements are translated into constraints on the CTS system designs. An important result in this section is that systems can be designed inside these constraints. Section 4 outlines the technical feasibility and describes in more detail the design and the engineering constraints of each system. Section 5 briefly describes an upgrade to the CTS diagnostic to permit fuel ion density ratio measurements with the same probe line and system front-end. Finally, Section 6 outlines future work needed to address issues related to the hardware and design.

ISSN 0106-2840
ISBN 978-87-550-3587-4

Contract no.:
EFDA Contract 01.654

Pages: 40
Figures: 29
References: 7

Information Service Department
Risø National Laboratory
Technical University of Denmark
P.O.Box 49
DK-4000 Roskilde
Denmark
~~Telephone +~~45 46774004
bibl@risoe.dk
~~Fax +45 46774~~013
www.risoe.dk

Contents

1 Introduction

The physics feasibility study in Ref. 1, explored the different frequency ranges which might be considered as candidates for fast ion collective scattering (CTS) diagnostics to provide spatially and temporally resolved measurements of the 1-D fast ion velocity distributions in ITER. The conclusion was that the 60 GHz option was the only system capable of meeting the ITER measurement requirements for the fusion alphas, with present or near term technology. This report is a preliminary study of the hardware design and engineering constraints for this frequency range.

Two separate systems make up the CTS diagnostic; one measuring the fast ion distribution parallel to the magnetic field and the other measuring that perpendicular to the magnetic field. This report is organized as follows: Section 2 conceptually describes the two systems and their main components. Section 3 clarifies the impact of design parameters such as beam widths and scattering angle on the CTS measurements. With this in hand, the ITER measurement requirements are translated into constraints on the CTS system designs. An important result in this section is that systems can be designed inside these constraints. Section 4 outlines the technical feasibility and describes in more detail the design and the engineering constraints of each system. Section 5 briefly describes an upgrade to the CTS diagnostic to permit fuel ion density ratio measurements with the same probe line and system front-end. Finally, Section 6 outlines future work needed to address issues related to the hardware and design.

Throughout this report the beam traces shown in the figures are from the beam simulations that represent the Gaussian beams by a bundle of rays consisting of 5 independent rays; the beam centre and 4 rays, each at one Gaussian half width from the centre.

2 Design summary

The fast ion CTS diagnostic proposed in the feasibility study report [1] consists of two separate systems. Each system has its own RF launcher and separate set of detectors. The first system measures the perpendicular component of the fast ion velocity distribution. It consists of radially directed RF launcher and receiver, both located in the equatorial port on the low field side (LFS). The receiver consists of a fixed quasi-optical mirror that measures backscattered radiation and couples it to a distributed set of receiver horns. This system will be referred to by the acronym LFS-BS system referring to the location of the receiver and the fact that it measures backscattered radiation. The second part of the CTS diagnostic measures the parallel component of the fast ion distribution. It consists of an RF launcher located in the mid-plane port and a fixed quasi-optical mirror mounted on the inner vessel wall that views the plasma from between two blanket modules. The mirror measures forward scattered radiation and couples it to a series of horns. This system will be referred to as HFS-FS referring to the location of the receivers and that they measure forward scattered radiation. The design of both LFS-BS and HFS-FS receivers is aimed at measuring at different spatial locations simultaneously with no moveable components near the plasma.

Figure 1 shows a 3-D view of the equatorial port #12 blanket with the apertures for the CTS in green. The LFS-BS launcher and receiver are located in the same poloidal plane. The HFS-FS launches radiation from the midplane of the port. As demonstrated in Ref 1, due to the constraints on the toroidal location of the receivers on the HFS, the toroidal location of the HFS-FS launcher is essential in achieving sufficient CTS signal and spatial resolution. The CTS diagnostic will share the port with the wide-angle viewing visible/IR system, H-alpha spectroscopy (upper edge view), and the visible continuum array. The apertures for these diagnostics are shown in blue.

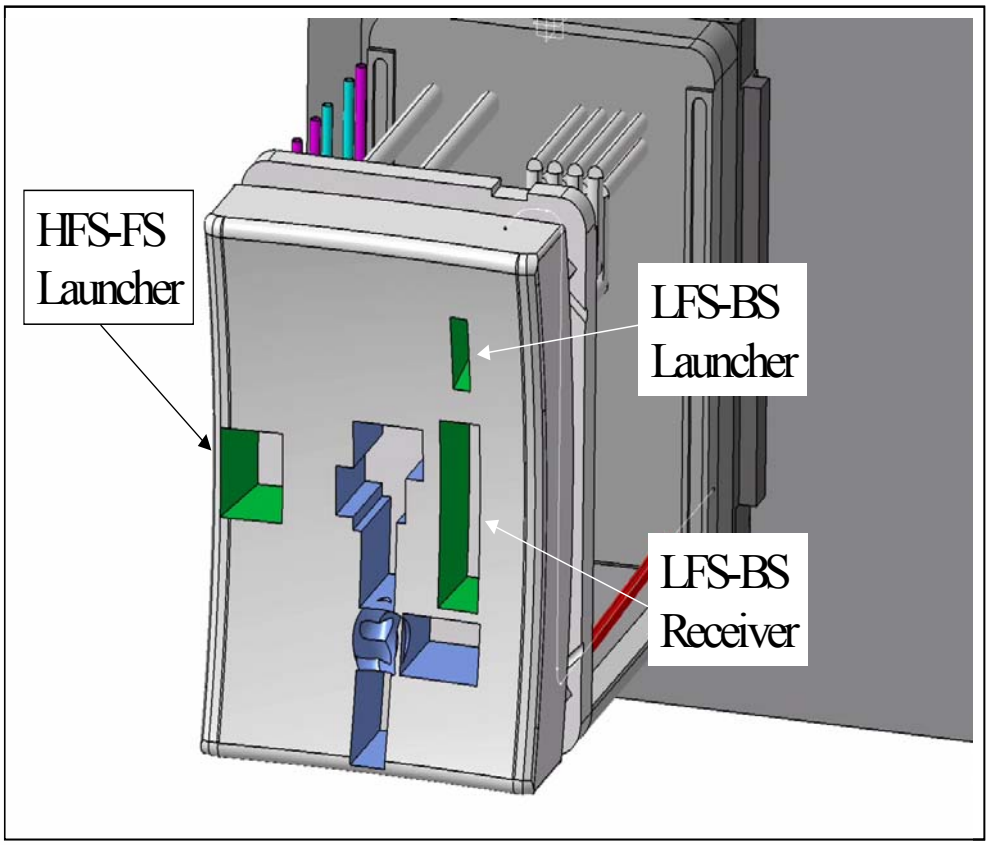

Figure 1. View from the plasma side of the mid plane port plug #12. The apertures for the CTS diagnostic are shown in green. The apertures in blue are for the other diagnostics that share the same port namely; wide-angle viewing visible/IR system, H-alpha spectroscopy (upper edge view) and the visible continuum array.

Figure 2 shows a top view of the transmission lines for the CTS diagnostic at the equatorial level of the tokamak building. Two high-power corrugated waveguides from the gyrotrons hall are directed to the equatorial port 12. Also shown schematically are the paths of the waveguides for HFS-FS (the upper port) and LFS-BS system (equatorial port). Both systems collect radiation from the plasma and transmit it through to the gallery toward the diagnostic hall.

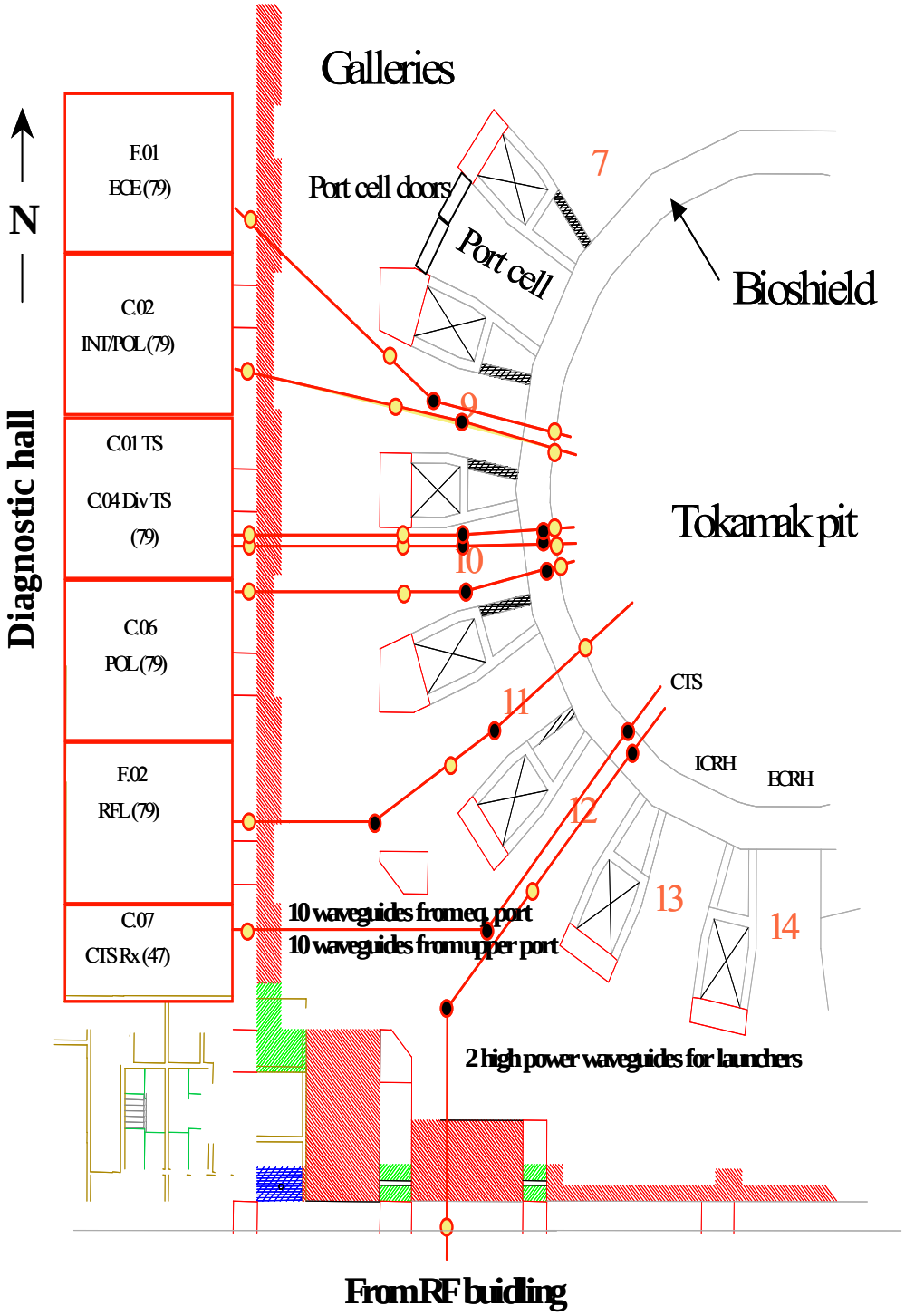

Figure 2. Top view of the equatorial level of the CTS's receiver and probe waveguide paths.

2.1 LFS backscattering system (LFS-BS)

The beam traces of the LFS-BS system for measuring the fast ion distribution perpendicular to the magnetic field are shown in Figure 3a where the probe and receiver antennae are in a mid-plane port. Optimisation of the positions and beam properties of the probe and receivers are described in the feasibility report [1]. Figure 3b shows a close up view of probe in black, one of the receiver beams in blue, scattering volume in red, and the resolved fluctuation vector, $\mathbf{k}^{\delta}$, in green. Note that the direction of the velocity space that is resolved is in the direction of $\mathbf{k}^{\delta}$. The beams and wave vectors are essentially in the poloidal plane, thus one can clearly see from Figure 3 that the fluctuation vector $\mathbf{k}^{\delta}$ is nearly perpendicular to the magnetic field.

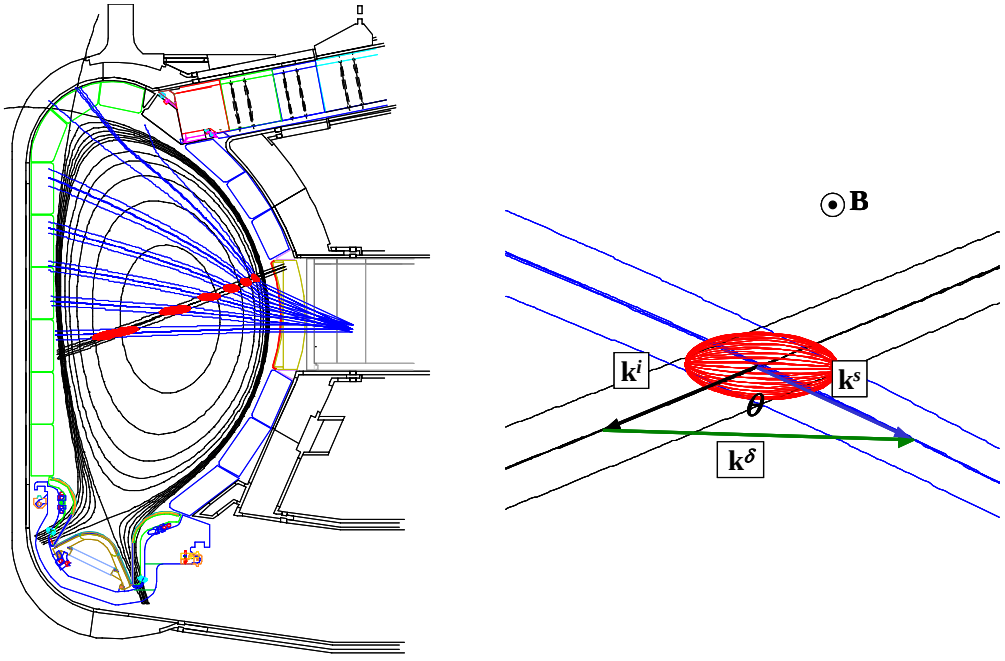

(a) **(b)**

Figure 3. Poloidal view of the LFS-BS set-up: (a) Beam traces of the LFS-BS system w.r.t the ITER vessel components. The probe is in black, receiver beam traces in blue, and the calculated scattering volume in red. (b): A close up view of the probe beam (black), one of the receiver beams (blue), the scattering volume (red). The drawing shows the wave vectors of the received scattered radiation $\mathbf{k}^{s}$, probe radiation $\mathbf{k}^{i}$, and the fluctuation wave vector $\mathbf{k}^{\delta}$. $\mathbf{k}^{\delta} = \mathbf{k}^{s} - \mathbf{k}^{i}$.

Figure 4 shows a schematic of the front-end of the probe launcher and the receiver of the LFS-BS system. The receiver consists of a quasi-optical mirror coupled to an array of horns mounted in a stainless steel frame that houses a series of fundamental wave guides connected to the horns. The waveguides are directed to tapers coupled to overmoded waveguides. Each horn is located at a different distance from the mirror and corresponds to a different radial position in the plasma as shown by the blue solid and dotted lines in Figure 4. The probe antenna consists of a waveguide supplying radiation to a Gaussian beam telescope (oriented in the horizontal direction) consisting of two quasi-optical mirrors.

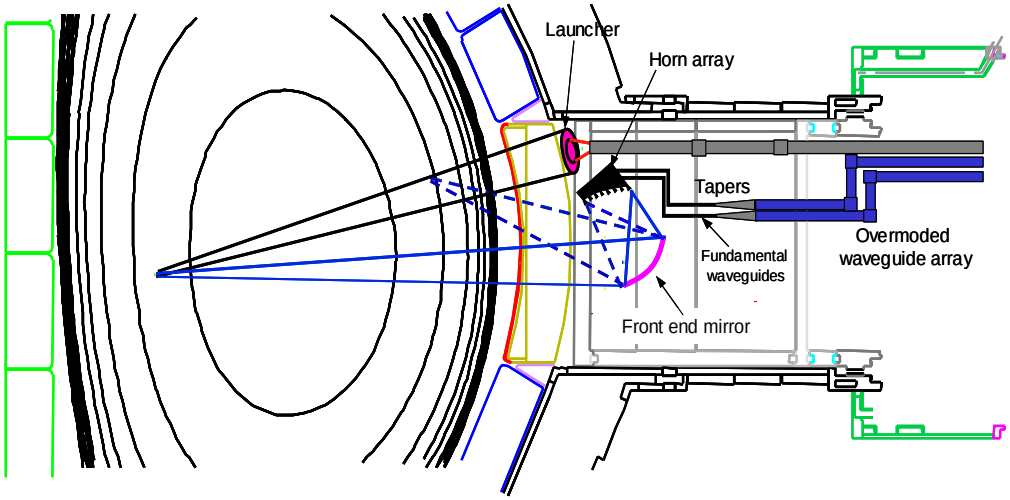

Figure 4. Schematic of the side view of the LFS-BS components. The probe launchers are located in the same poloidal plane as the detectors.

2.2 HFS forward scattering system (HFS-FS)

The beam traces of the CTS HFS-FS set-up are shown in Figure 5a. It shows the location of the probe and receivers with respect to the ITER port plug and blanket. The probe is located in the mid-plane port on the LFS and the detectors are located on the HFS viewing the plasma from between the blanket modules. The beam traces from the receivers and probe are shown in blue and black respectively. For clarity, only 5 receiver beams are shown. This configuration measures the velocity distribution near parallel to the magnetic field as shown by the wave vectors in Figure 5b.

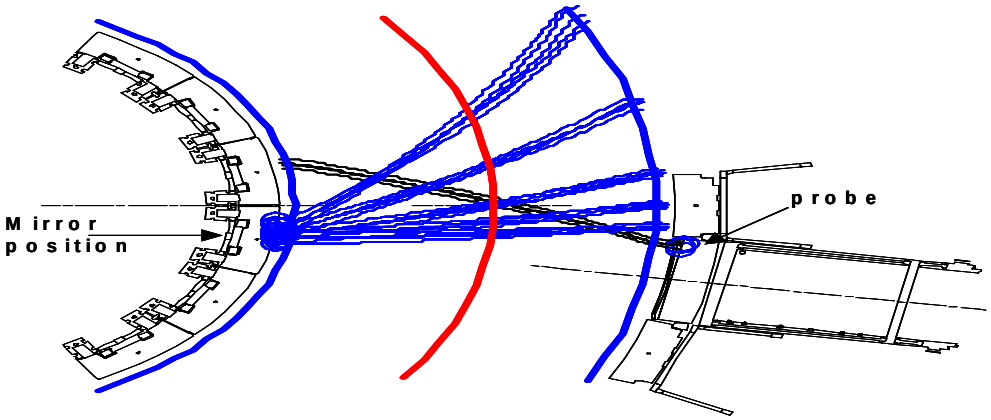

(a)

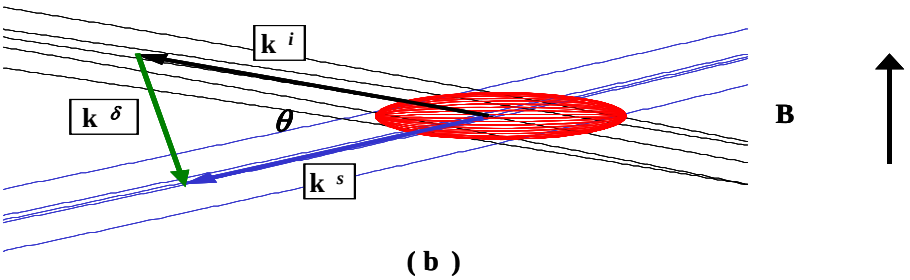

(b)

Figure 5 (a). Top view of beam traces for the HFS-FS with a LFS probe launcher (black) and HFS detectors (blue). The red curve indicates the plasma centre. (b) Close up view of the probe beam and one of the receiver beams with the scattering volume in red. Shown are the wave vectors of the received scattered radiation $\boldsymbol{k}^s$, the incident probe radiation $\boldsymbol{k}^i$, and the fluctuation vector $\boldsymbol{k}^\delta = \boldsymbol{k}^s - \boldsymbol{k}^i$ which is near parallel to $\boldsymbol{B}$.

The hardware of the HFS receivers consists of a quasi-optical mirror mounted on the inner vessel wall below the blanket module key as shown in the side view sketch in Figure 6a. Toroidally the mirror is located between the cooling manifolds (Figure 6b). The mirror collects scattered radiation from between blanket modules and couples it to a series of horns. The horns are distributed toroidally, each representing a different toroidal angular view in the plasma. The horns are encased inside a cast, housing fundamental waveguides that are routed upwards along the inner vessel wall. These are in turn coupled to over-moded waveguides that run up along the vacuum vessel wall behind the blanket modules toward the upper port. Note that a 30 mm vertical distance between the blankets shown is needed. This is discussed in section 3.2.

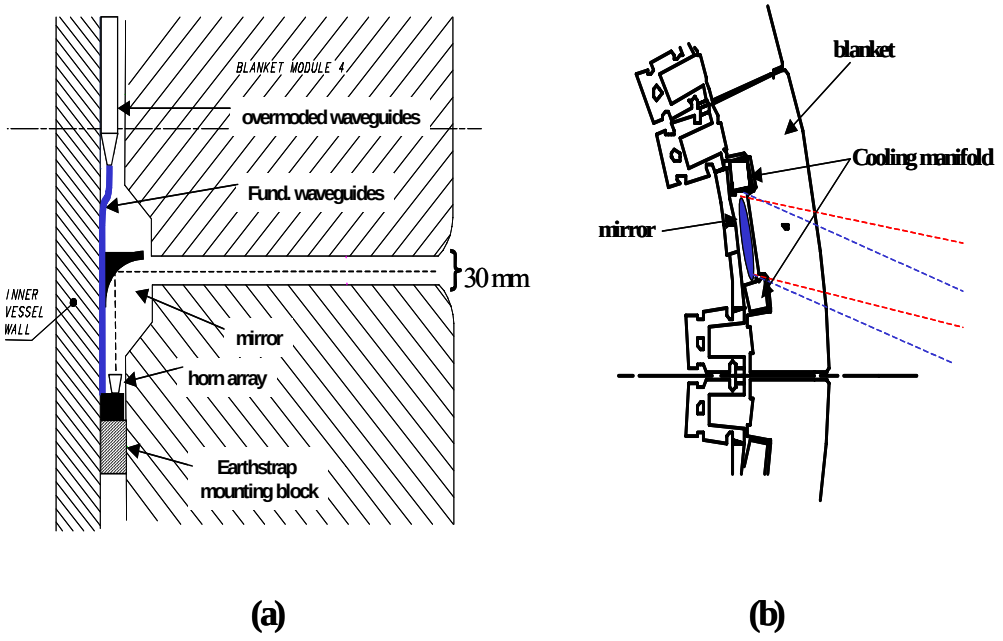

Figure 6 (a). Cross section of blanket modules 3 and 4 with mirror, horn array, and waveguide assembly. The vertical distance between the blanket modules gap diameter is 30 mm as shown. (b) Top view of mirror located behind the blanket module between the cooling manifolds.

3 Function and design requirements

In the physics feasibility study [1], the choice of scattering geometry was optimised. The optimisations are primarily driven by the need to satisfy requirements on; resolving power, spatial resolution, and robustness all at a broad range of plasma parameters. The resolving power was defined and discussed in Ref 1 section 1.8. It is a measure of the accuracy with which the system can estimate the fast ion velocity distribution for a given velocity space resolution. For all systems discussed in this report, a minimum resolving power of 4 is selected. This corresponds to requiring that the systems resolve at least L^2 = 16 orthogonal components of the fast ion velocity distribution, essentially points in, the fast ion distribution, with an uncertainty, σ, smaller than the target accuracy, $\Delta = 6\times10^9 s/m^4$. Another requirement is that the spatial resolution should allow 10 spatially localized non-overlapping measurements across the plasma radius. Finally, the measurements must be robust against variations in plasma parameters and dispersion effects.

The diagnostic requirements have a direct implication for which beam parameters are acceptable, and hence on the design of both the probe and receiver antennae. It is important to clarify how the beam properties influence the criteria mentioned above. The resolving power, L, is directly proportional to beam overlap, O_b, that accounts for the effects of the widths of the probe and receiver beam patterns and the extent to which they overlap in the plasma. The optimisations, for each scattering geometry, consist essentially of a compromise between the beam overlap, the scattering volume size (that determines the radial resolution), and the robustness. This is covered in greater detail in section 1 of Ref. 1.

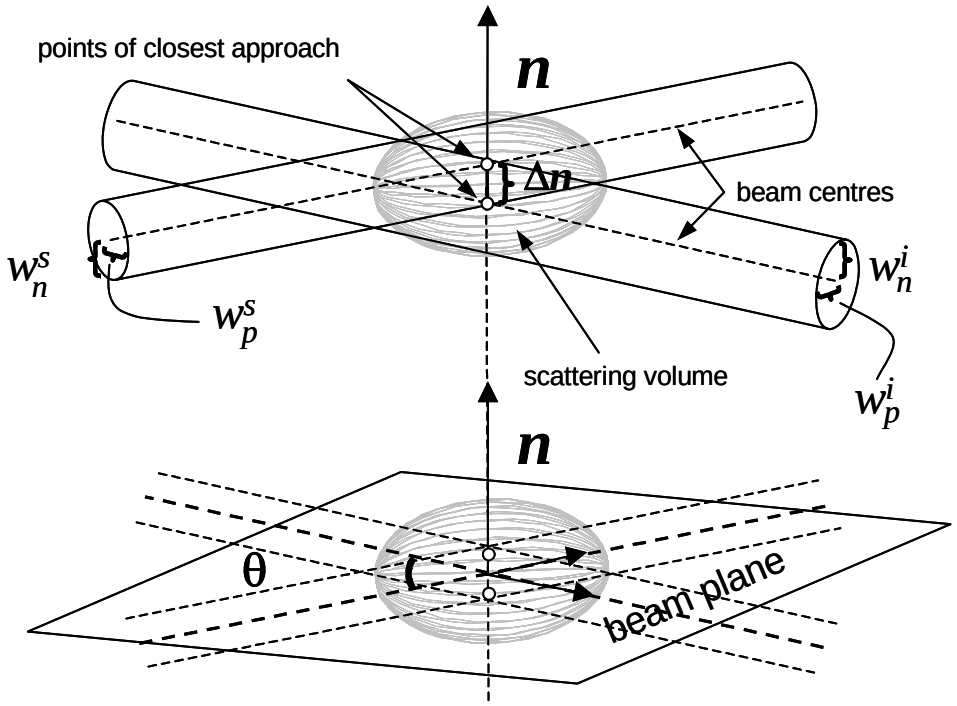

Figure 7. Schematic presentation of two intersecting beams and the scattering volume. The vector ***n***, defined by the two points of closest approach, is normal to the *beam plane* which includes the centre of the scattering volume. The beam widths w_n and w_p are normal and parallel to the beam plane respectively. The angle between the beam vectors is θ. The superscript *i* and *s* refer to the incident beam (probe) and the beam of received scattered radiation (receiver), respectively.

Figure 7 shows a schematic presentation of two intersecting beams and the scattering volume defined as the smallest volume from which 90% of the received scattered radiation comes. The superscript *i* and *s* refer to the incident beam (probe) and the beam of received scattered radiation (receiver) respectively. The *beam plane* is the plane that includes the centre of the scattering volume and is spanned by the direction vectors of the two beams. The vector ***n*** is normal to this plane and parallel to the line through the two points of closest approach of the beam centre lines. The beam widths w_n and w_p are the widths normal and parallel to the beam plane respectively. In the report [1] we recalled that the expression for the beam overlap for Gaussian beams is

$$O_b = \frac{1}{|\sin(\theta)|} \frac{2}{\sqrt{2\pi\left(\left(w_n^i\right)^2 + \left(w_n^s\right)^2\right)}} \exp\left(-\frac{2\Delta n^2}{\left(w_n^i\right)^2 + \left(w_n^s\right)^2}\right).$$

We see from this expression that θ, Δn, and w_n affect beam overlap and hence the CTS signal. Here is an outline to summarize the effects of the individual variables.

θ	The scattering angle which is the angle between the beam vectors. Decreasing θ results in a long scattering volume, which increases the CTS signal, but reduces the spatial resolution.
Δn	Distance of closest approach between the beam centres. It is clear that the CTS signal is maximized when the beam centres intersect ($\Delta n = 0$).
w^i_n, w^s_n	Beam widths perpendicular to the beam plane. The CTS signal increases as the beam widths perpendicular to the beam plane decrease. The spatial resolution is only weakly affected by these parameters for the scattering geometries considered here.
w^i_p, w^s_p	Beam widths parallel to the beam plane. Modifying beam parameters parallel to the beam plane does not affect the CTS signal, but does affect the spatial resolution.

The locations of the probe and receiver with respect to each other determine θ and Δn, whereas the design of the launcher and receiver front-ends determine the beam widths w^i_n, w^s_n, w^i_p, and w^s_p. Referring to Figure 3 and Figure 5, the beam plane for the LFS-BS system lies more or less parallel to the poloidal plane whereas for the HFS-FS system the beam plane lies more or less parallel to the horizontal plane.

3.1 Design requirements for the LFS-BS system

Figure 3a shows the beam traces of the probe and the receivers for the LFS-BS system. The beam shape needed for this system is sketched in Figure 8. The beam widens in the horizontal direction for robustness and is focused in the vertical direction to improve the radial resolution. Recall that for the LFS-BS system, the horizontal beam diameter determines CTS signal strength and the vertical beam diameter determines the radial resolution. Focusing the beam in the vertical direction (reducing w_p) reduces the scattering volume and hence improves the radial resolution. Studies have shown that the vertical diameters of the probe and receiver beams should be of the order of 100 mm in the plasma to ensure sufficient radial resolution [1]. In addition, the studies have shown that the CTS signal strength is sufficiently large that it can tolerate reduction by widening the beam width in the horizontal direction (w_n) to ensure robustness.

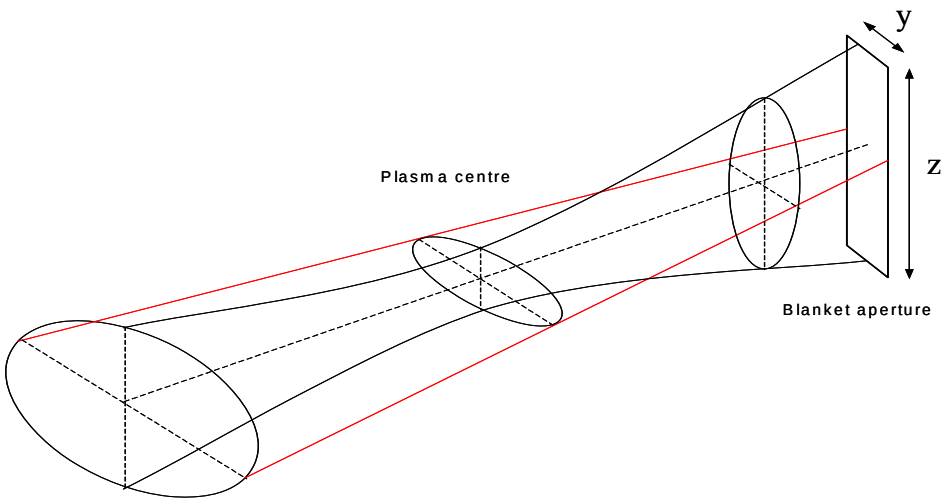

Figure 8. Three-dimensional sketch of a LFS-BS beam viewed from the plasma. At the plasma edge the beam is focused in the vertical plane and diverging in the horizontal plane. The beam shape has been exaggerated for illustration purposes.

Robustness includes tolerance to mechanical imperfections and tolerance to refraction that varies with frequency (dispersion) and density. The probe and receiver beams do not follow the same trajectories and generally do not have the same frequency, hence they refract differently. This affects both the location of the scattering volume where the measurement is taken, and the beam overlap. We refer to the former as positional robustness and the latter as beam overlap robustness.

The positional robustness does not improve by widening the beams. In the present geometry with the reference plasma ($n_e(0) = 1.0 \times 10^{20}$), the radial variations, due to density fluctuations of 10% and due to dispersion, vary between 3 % and 5 %.

Widening of the beams in the horizontal direction does improve the beam overlap robustness especially against dispersion effects. The beams need to be wide enough to ensure that changes in refraction do not cause significant variation of the overlap but still sufficiently narrow to maintaining an adequate value for the overlap and hence the CTS signal strength. The system is optimised to be robust against fluctuations in density of ±10% and against dispersion over the full spectral width of the fast ion feature. Depending on the radial location of the measurement, the spectral half-width for the LFS-BS system is 2.4 – 4.5 GHz [1], corresponding to a relative frequency variation of 4% to 8%. For the LFS-BS system the considered frequency variation has a larger impact on refraction and hence robustness than does the considered density variation.

A divergence angle of 2° is the best compromise between CTS signal strength and robustness for a wide range of plasma densities. The question arises as to whether it is advantageous to widen both the probe and receiver beams. Figure 9 compares the resolving powers obtained with receiver beams which are respectively diverging and non-diverging in the horizontal direction. The results are for the reference ITER plasma with a central electron density of $n_e(0) = 1.0 \times 10^{20}$ m^{-3}. Figure 10 shows the same comparison except for a lower density of $n_e(0) = 0.7 \times 10^{20}$ m^{-3}. The results show that horizontally diverging receiver beams in the plasma reduce the resolving power. This reduction of resolving power is acceptable for the density of $n_e(0) = 1.0 \times 10^{20}$ m^{-3} but not for lower densities at $n_e(0) = 0.7 \times 10^{20}$ m^{-3}. In conclusion, a divergence angle of 2°, only for the probe beam, improves the robustness against dispersion while still maintaining a sufficient CTS signal for lower densities.

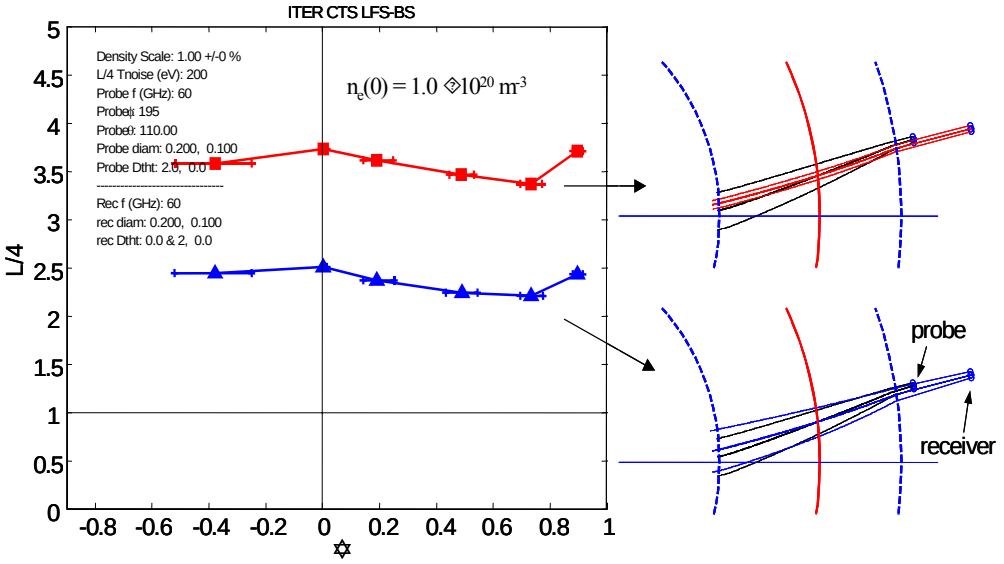

Figure 9. (a) Resolving power / 4 versus the magnetic surfaces, where the centre of the scattering volume is located. The results are for the ITER reference plasma ($n_e(0) = 1.0 \times 10^{20}$m^{-3}). Each plotted point corresponds to a receiver beam plotted in Figure 3a. The red and the blue curve represent the same configuration except that the horizontal divergence angle for the receiver beams is 0° for the red curve and 2° for the blue. (b) Top view of the probe in black and receiver beam. The top picture shows a receiver beam in red with a horizontal divergence angle of 0° while the bottom picture shows a receiver beam in blue with a divergence angle of about 2°.

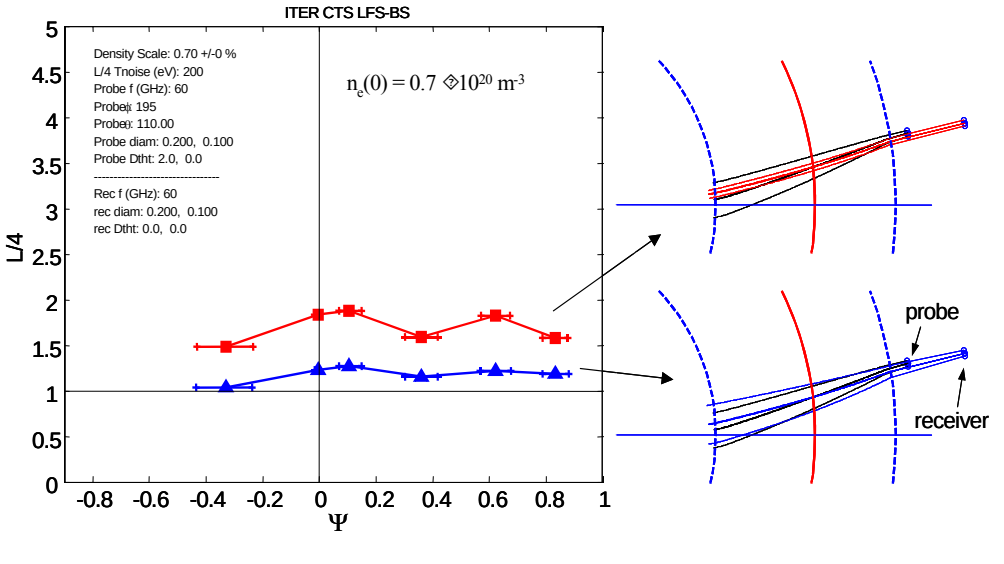

Figure 10. Same as Figure 9 except that the central electron density is $n_e(0) = 0.7 \times 10^{20}$ m.

Achieving the probe and receiver beam properties in the vertical and in the horizontal directions described above constrains the design of the launcher and receiver front-ends and sets minimum requirements on sizes of the front-end mirrors and blanket apertures. Fundamentally these constraints stem from the fact that there is a lower limit to the beam size that can be projected a given distance from a given aperture or mirror. Figure 11,

Figure 12, and Figure 13 show Gaussian beam diameters1 as functions of distance along the beams. The beams in each figure differ in their radii of curvature at the front-end mirror. The three figures show the results for mirror dimensions of 450 mm, 300 mm, and 200 mm respectively. Figure 11 and Figure 12 present calculations relevant to achieving vertical widths of receiver beams in the range of 100 mm at their intersections with the probe beam. Figure 13 presents calculations relevant to the horizontal beam widths.

The vertical black line in each graph represents the aperture at the blanket module. It should be noted that in the vertical direction the blanket aperture for the receiver is mainly determined by the range of viewing directions required for radial coverage of the plasma. The front-end receiver mirror is retracted from the blanket among others to decrease the angle between receiver beams and the density gradient for all viewing direction required for a wide radial coverage. Decreasing this angle reduces the refraction of the beams. In the preliminary design, the first mirrors of the probes and the receiver are located 600 and 1200 mm respectively behind the plasma facing surface of the blanket. Engineering constraints revealed in future studies may limit this distance. Therefore a reference distance of 1 m will be used in this section.

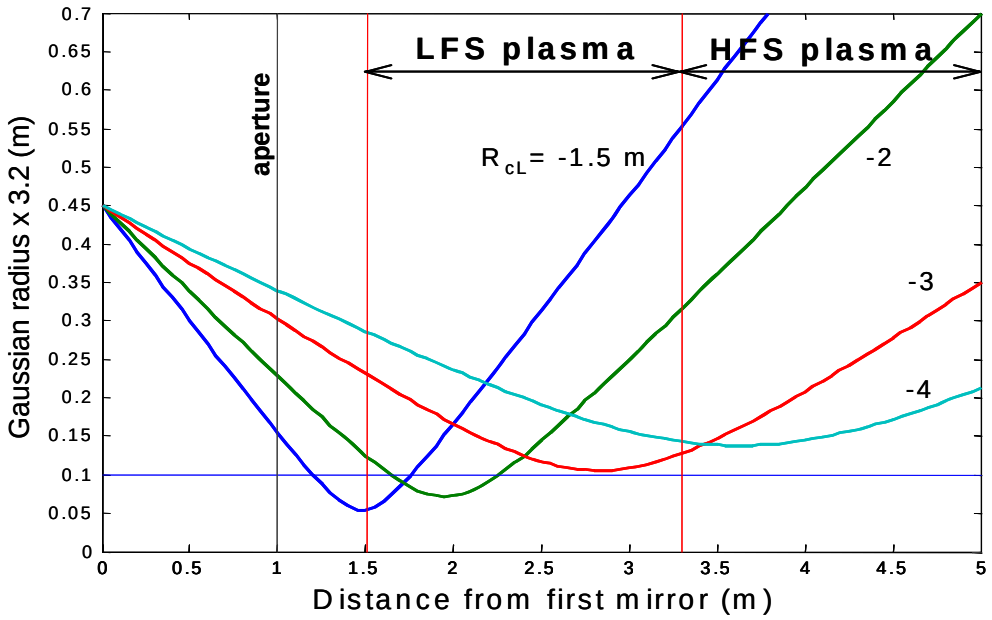

Figure 11. Beam diameters (Gaussian radius × 3.2) as functions of distance from front-end mirror. The curves are for different radii of curvature, R_{cl}, (in meters) at the mirror. The negative values of the radii of curvature indicate that the beams are focusing toward the plasma. The vertical red lines represent the position of the boundaries of different plasma regions. The vertical black line represents the position of the blanket aperture. The mirror size is 450 mm and the frequency of the gaussian beam is 60 GHz.

The vertical red lines in each graph bound the plasma regions. These graphs set lower limits on the mirror dimensions and the aperture sizes needed to produce the beams described above. The mirror size in each graph represents the minimum value at which the required beam properties can be achieved.

1 The Gaussian half-width *w* on the ordinate of the graph is multiplied by 2×1.6 to represent the beam diameter (*Db* = *w* × 2 × 1.6) which includes 99.4 % of the total power.

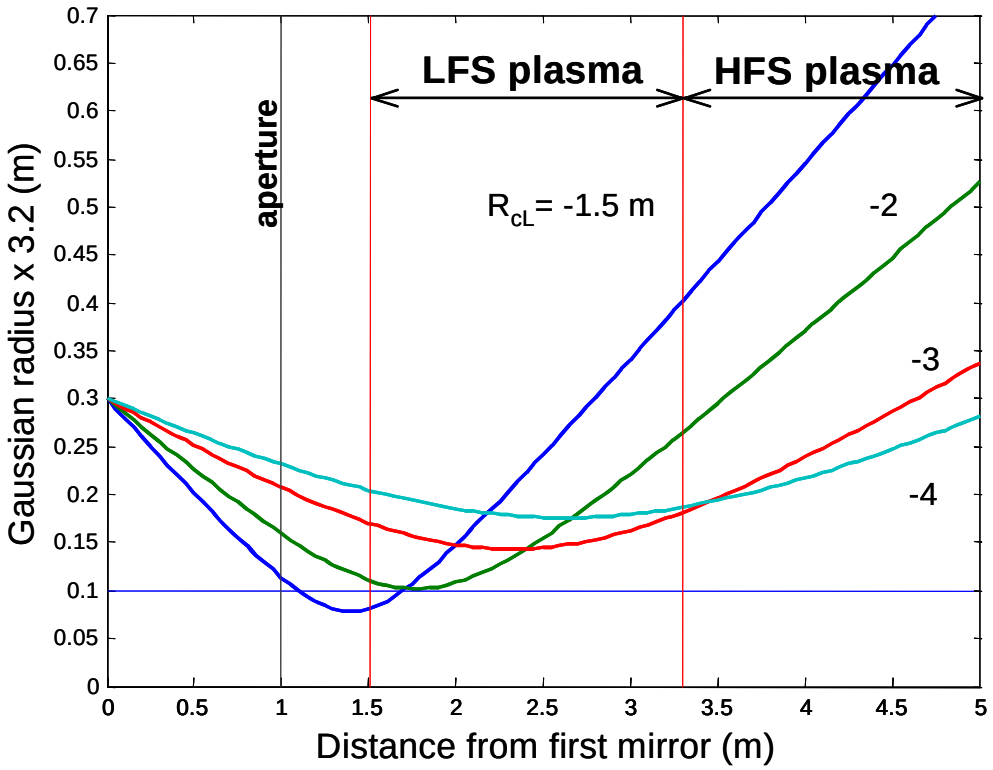

Figure 12. Same as Figure 11 except for mirror size of 300 mm.

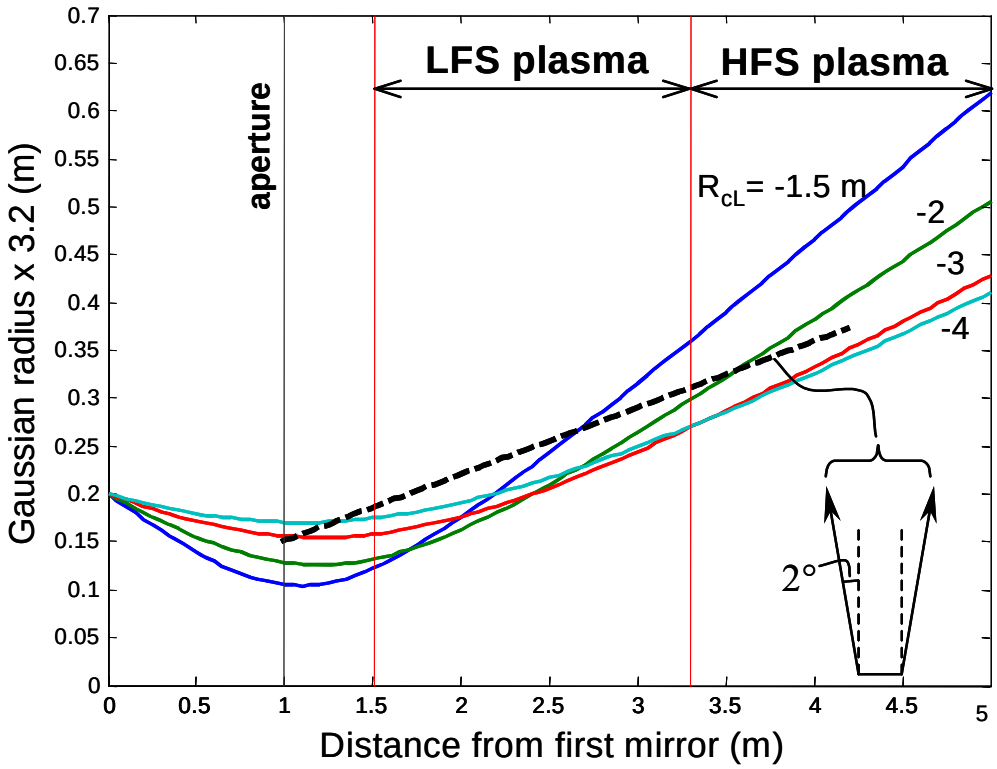

Figure 13. Same as Figure 11 except for mirror size of 200 mm. The slope of the dashed black line in the graph represents the rate of increase of the distance between two rays, each having a divergence angle of 2° from the parallel direction.

With reference to Figure 11, Figure 12, and Figure 13 we can identify the beams which best meet our requirements and thus set lower limits on required sizes for front-end mirrors and blanket apertures.

Launcher: For the probe we require that the vertical beam diameter is less than 200 mm and that it is widening horizontally with a divergence angle of 2°. The beam that satisfies this criterion in the vertical direction is shown as the red curve in Figure 11. Its radius of curvature at the mirror, R_{cL}, is –3 m. The required beam property in the horizontal direction is shown in Figure 13. The slope of the dashed black line in Figure 13 graph represents the rate of increase of the distance between two rays, each having a divergence angle of 2° from the parallel direction. The Gaussian beam that needs the smallest aperture and matches this divergence has a radius of curvature $R_{cL} \approx$ -3 to -4 m. In summary, if the first mirror is located 1 m from the aperture, its dimensions should be at least 200 H × 450 V mm viewing through an aperture with dimensions greater than 150 H × 300 V mm.

Receiver: For the receiver beams we require that the vertical beam diameters are less than 100 mm where they intersect the probe. In the horizontal direction we require that the diameters are less than 200 mm at the intersections with the probe. The set of beams shown in Figure 11 are close to meeting the requirements. The waists are intended to be at the locations of the intersections with the probe. The beams with waists in the low field side of the plasma more than meet the requirement. The beam with its waist on the high field side of the centre is too wide. Achieving the goal here requires a mirror of approximately 550 mm. Placing the beam waist of each beam at a different radial position in the plasma using the same front-end mirror is achieved by varying the distance between the mirror and each receiver horn as illustrated in Figure 4. The distribution of viewing angles and hence the locations of the scattering volumes shown in Figure 3 are determined by the poloidal distribution of the receiver horns shown in Figure 4. The vertical size of the aperture of 720 mm is determined by the required radial coverage where the receiver beam pivot point is located at the front-end mirror. The required beam property in the horizontal direction for the receiver beams is shown in Figure 12. As mentioned previously, to ensure the required CTS signal for lower densities, the receiver beams' horizontal dimensions should be < 200 mm inside the plasma, which corresponds to beams with $-4 \text{ m} < R_{cL} < -3$ m. In summary, to satisfy the measurement requirements, the receiver first mirror at 1 m from the blanket has dimensions 300 H × 450 V mm viewing through an aperture with dimensions greater than 200 H × 720 V mm.

3.2 Design requirements for the HFS-FS system

Figure 5a shows the beam traces of the probe and the receiver beams for the HFS-FS system. In this set-up, we recall that the beam plane is near parallel to the horizontal plane. Therefore, horizontal beam properties govern spatial resolution, and vertical beam dimensions govern CTS signal and robustness.

Launcher: The launcher in the HFS-FS system, focuses the beams in the horizontal and vertical direction to produce the required probe beam. The beam diameter of the probe should be less than 200 mm in both directions to satisfy the measurement requirements [1]. Due to the variations in the scattering angles, the scattering volumes are smaller on the HFS and hence the radial resolution is better on the HFS. Therefore, the probe beam waist in the horizontal direction is best placed in the LFS region of the plasma. The beam with $R_{cL} \approx$ -3 m in Figure 11 satisfies the criteria for both directions. As with the LFS-BS launcher, the distance between the first mirror and the aperture is limited to about 1 m. At this distance the mirror dimensions should be at least 450 H × 450 V mm viewing though an aperture with size of 300 H × 300 V mm.

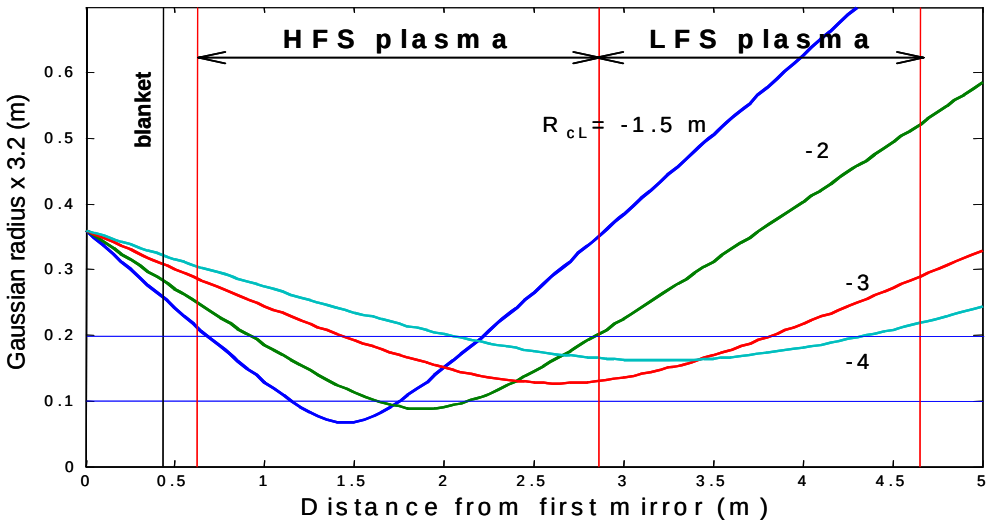

Figure 14. Beam diameter (Gaussian radius × 3.2) as functions of distance from mirror for different radii of curvature, R_{cl}, (in meters) at the mirror. The vertical red lines represent the position of the boundaries of different plasma regions. The vertical black line represents the position of the blanket. The mirror size is 360 mm and the frequency of the Gaussian beam is 60 GHz. The negative values of the radii of curvature indicate that the beams are focusing toward the plasma.

Receiver: The constraints in Figure 6b limit the horizontal dimension of the receiver mirror to 360 mm. This determines the radial resolution for the system. The studies in Ref 1 have shown that beam diameters less than 200 mm in the horizontal direction are needed to achieve the require radial resolution. Figure 14 shows the Gaussian beam diameters as functions of distance from the first mirror on the HFS. The graph shows the possible beam dimensions which can be achieved in the horizontal direction with a horizontal size of the mirror of 360 mm.

The vertical beam properties, which govern the beam overlap and hence tha CTS signal strength, depend on the vertical dimension of the gap between the blankets. The radiation pattern between the blanket modules was studied [1]. The receiver beam vertical divergence angle α is inversely proportional to the distance between the blankets. Figure 15, Figure 16, and Figure 17 show beam traces and corresponding resolving powers for vertical distances between blanket modules of 14 mm, 20 mm, and 30 mm respectively. The left graph (a) of each figure shows the poloidal cross section of the equilibrium and the beam traces of the receivers (in blue) and the probe (in black). The figures clearly show how the vertical gap between the blankets affect the vertical divergence angle of the receiver beam. This determines the beam width normal to the beam plane (w_n) and thus has a direct consequence on the CTS signal strength. The right graph (b) of each figure shows the resolving power for different plasma densities, plotted against the radial location of the scattering volume. From these results we find that in order to satisfy the ITER measurement requirements for the range of plasma densities from $n_e(0) = 0.7\times10^{20}$ m^{-3} to $1.2\times10^{20}m^{-3}$, the vertical distance between the blanket modules in this port must be at least 30 mm.

From Figure 6a we note that the blanket module key above the mirror limits the position of the mirror. Therefore, only the vertical dimensions of the lower blanket need to be modified.

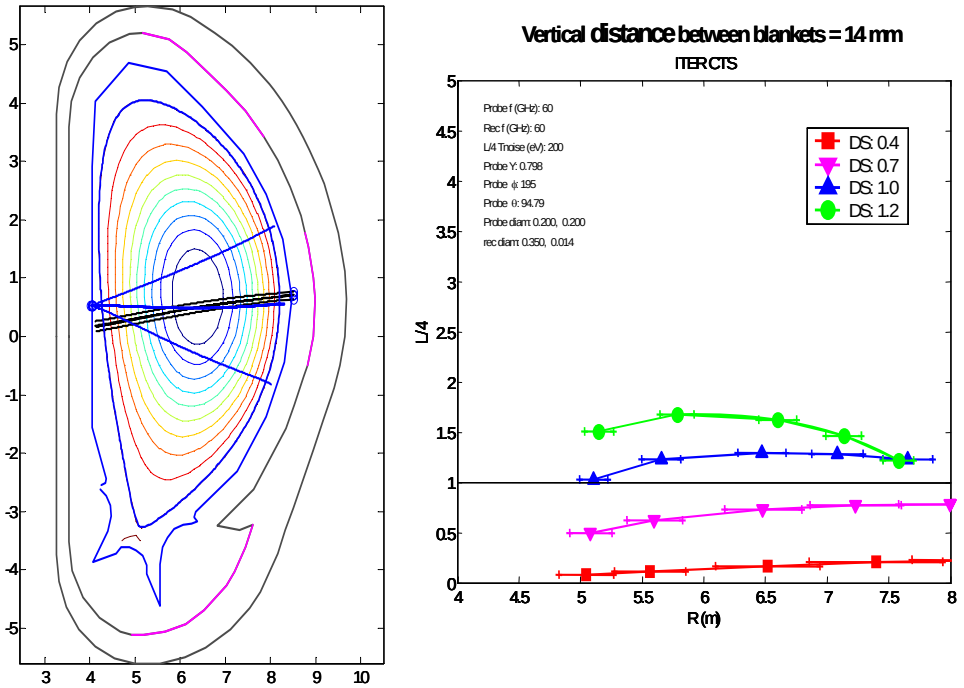

(a) **(b)**

Figure 15. Beam traces and resolving powers for HFS-FS system with a vertical distance between blanket modules of 14 mm at receiver slot. (a) Poloidal cross section of the equilibrium and the beam traces of a receiver (in blue) and the probe (in black). (b) The resolving power / 4 for different plasma densities plotted against the radial location of the scattering volume.

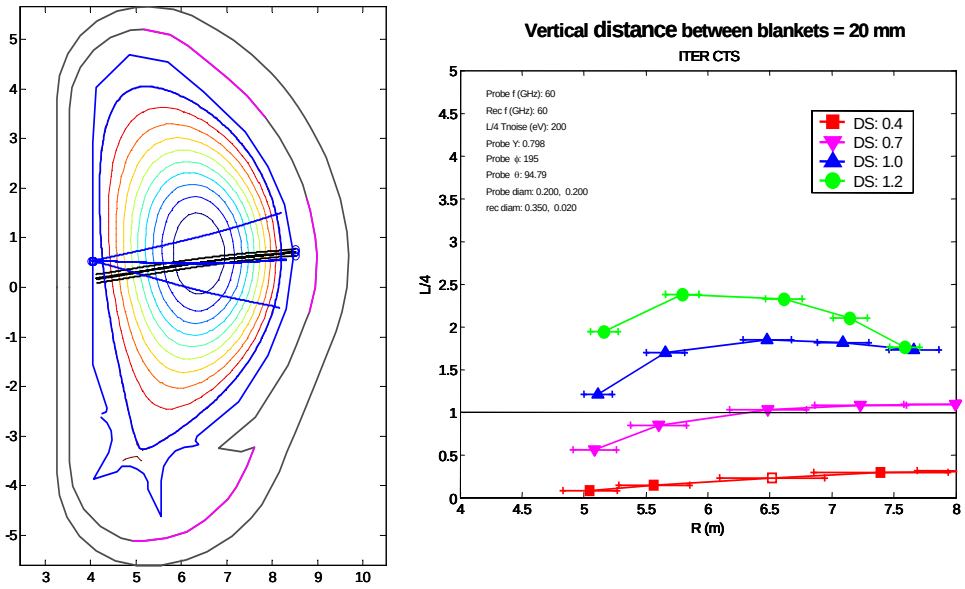

(a) **(b)**

Figure 16. As Figure 15 only here for a vertical distance between blanket modules of 20 mm.

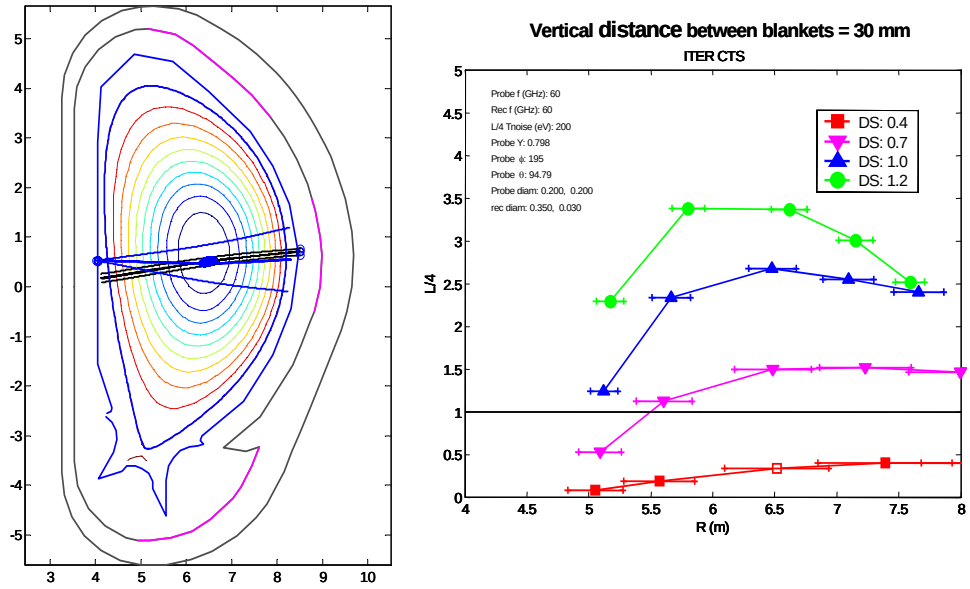

(a) **(b)**

Figure 17. As Figure 15 only here for a vertical distance between blanket modules of 30 mm.

4 Design description

This section describes the preliminary phase of the hardware design for the CTS diagnostic. The CTS diagnostic will share port #12 with the following diagnostics; visible and IR wide angle and divertor viewing, D_α spectroscopy (design similar to divertor viewing but looking upwards) and visible continuum array. Preliminary analysis has shown no integration problems with the other diagnostics in port #12. The design includes front-end components and waveguide systems of the HFS-FS receiver installed on the vacuum vessel wall in a manner similar to those of the plasma position reflectometry diagnostic [2]. The waveguides for the HFS-FS receiver are routed upwards along the inner vessel wall toward the upper-port #12 where the upper ECH launcher is located. The space needed for the HFS-FS waveguides is small and is not expect to interfere significantly with the existing designs.

The design description is divided into three main parts. The first describes the launchers for the LFS-BS and HFS-FS systems, the second part describes the receiver of the LFS-BS system, and the third section describes the receiver of the HFS-FS system. Figure 18 shows the layout of the CTS system in port #12 with the different transmission line sections. Like all other diagnostics on ITER, the CTS hardware is composed of sections that have to comply with varying sets of ITER engineering requirements.

- In-vessel front-end quasi optical antenna system.
- In-vessel inboard waveguide system (applies only to HFS-FS receiver)
- Port plug waveguide system (applies to launchers & LFS-BS receiver)
- Port inter-space transmission system
- Port-cell transmission system
- Gallery transmission system
- Acquisition system in diagnostic hall (receivers)
- Gyrotrons and transmission lines in RF building (probes)

All components in the port plug are cooled by water from the blanket primary heat transfer system. Additional mitre bends of the waveguides in the port plug will be

implemented as needed pending analysis of fast neutron streaming in the waveguide channels. The in-board components of the HFS-FS receiver are cooled by the vacuum vessel through conduction. Due to the baking temperatures of about 240° C, the main material used for the in-vessel components is stainless steel. All waveguides in the port plug need to be disassembled at the port plug back flange.

The port inter-space, shown in Figure 18, is bounded by the *port plug flange* (sometimes referred to as the port back plate) and the *cryostat*. The primary vacuum boundary is usually located at a window just outside the plug back flange. The second vacuum boundary is located at a second window just outside the bioshield. Hence the port inter-space usually houses the second vacuum boundary. All the movement compensation units for the waveguides are enclosed within the port inter-space area. The movement compensation units are designed to accommodate movements of the vessel with respect to the bioshield. The radial and vertical (R,Z) displacements from room temperature to operating temperature (120° C) are expected to be about (18 mm, 2 mm) at the equatorial level and (18 mm, 10 mm) at the upper level.

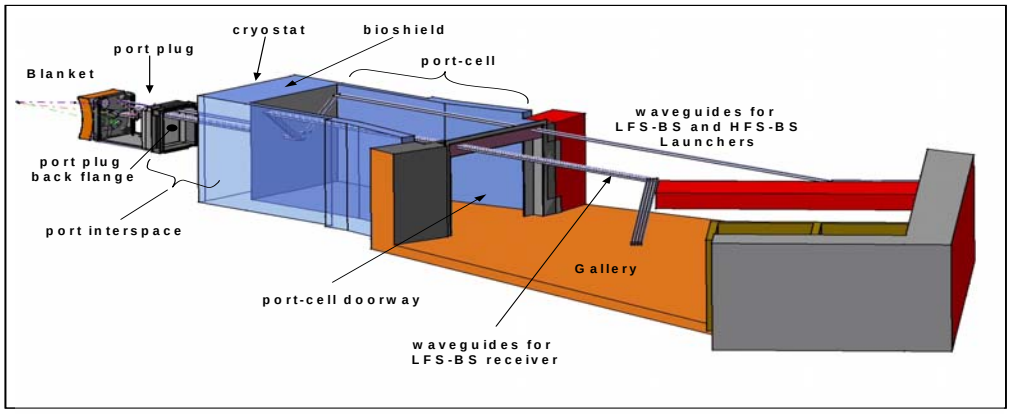

Figure 18. Preliminary CTS diagnostic design. Sections of the CTS transmission line from port plug #12.

The port-cell is bounded by the bioshield and the port-cell door. To minimize the amount of waveguides to be dismantled during port plug access, the waveguides just outside the boishield are directed upwards via mitre bends as shown in Figure 18. The waveguides are then directed out above the port cell door toward the gallery where they are directed toward the diagnostic hall.

4.1 Probes

The preliminary phase of the design of probes is based on studies performed for the ECH&CD system [3]. Each probe consist of launcher front-end optics, an RF power generator (gyrotron), a transmission line to transmit the RF power from the gyrotron to the launcher, and a power supply. The main components in each section are listed in the table in Appendix A.1;

4.1.1 Front-end quasi optics

Figure 19 shows a 3-D view, from the plasma, of the CTS system in port #12. The blanket module has been removed and the plug front plate was made semi-transparent in this illustration for a better view of the front-end optics and the port plug waveguides. The launcher for both the LFS-BS and HFS-FS system consists of two fixed quasi-optical ellipsoidal mirrors fed by a corrugated high power waveguide.

The purple dash-dotted line shows the beam centre of the LFS-BS probe. The two front-end mirrors are displaced toroidally relative to each other and are at the same vertical

position. The first mirror is located just behind the blanket above the LFS-BS receiver. As mentioned in Section 3, the mirrors for the launcher are ellipsoidal and designed to produce non-circular beams. From the preliminary analysis, the vertical and horizontal dimensions of the first LFS-BS mirror should be at least about 200 H × 450 V mm. The first and second mirror is located radially about 0.5 m behind the blanket plasma facing surface which corresponds to the plug front plate location.

Shown as an orange dash-dotted line, is the beam centre of the HFS-FS probe. The two front-end mirrors are offset vertically. The dimensions of the first mirror should be at least 300 H × 400 V mm. The distance between the blanket plasma facing surface and the first and second mirror is about 1.2 and 0.5 m respectively.

Further analysis of the engineering constraints need to be done to determine the final dimensions and locations of the launcher front-end optics.

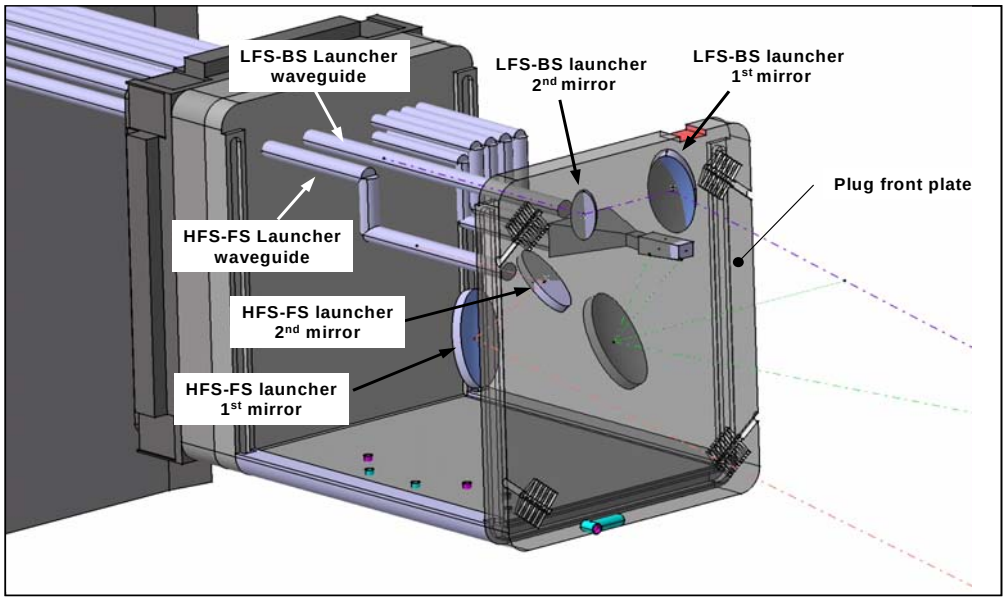

Figure 19. Design of the CTS components in port plug #12 viewed from the plasma without the blanket.

Not shown in Figure 19 are the details of the support and cooling structures for the front-end which need to be addressed in the next phase of the design. The requirements for the front-end mirrors are 1) to withstand heat loads from the plasma expected to be 0.2 MW/m^2 in the form of electromagnetic radiation and 1.0 MW/m^3 in the form of neutron stream heating, and 2) to have sufficient flexibility to accommodate the resulting thermal stresses. Most of the launcher is cooled by the *blanket primary heat transfer system water*. As with the ECRH launcher, the material used for the mirrors is a stainless-steel body with a thin copper alloy layer.

4.1.2 Transmission lines

The transmission lines for the probes require standard components similar to the ECH&CD system. The transmission lines are overmoded corrugated circular waveguides. The waveguides in the port plug and in the inter-port space are fabricated from stainless steel material and lined inside with copper. Aluminium cannot be used for the waveguides inside the cryostat because of the 240 °C baking temperature. The dimensions are the not yet entirely determined. The most suitable waveguide for ITER has an inner diameter of 63.5 mm capable of operating over the range 50 to 220 GHz. There is an open issue on whether such waveguides will need to be water-cooled for ITER.

Figure 20 shows the top view of the CTS front-end optics and the waveguides. The figure shows the relative distance of the launcher waveguides to the LFS-BS receiver waveguides. The figure also shows the toroidal angle between the launch direction and radial direction for each system. An angle of about 10° for the HFS-FS probe is needed for optimisation of the CTS signal. The LFS-BS system launches at an angle of about 5°. For the LFS-BS system the finite toroidal launch angle is introduced to avoid having the resolved fluctuation wave vector perpendicular to the magnetic field. This prevents the fast-magnetosonic wave from entering the CTS spectrum, which would make it impossible to estimate the fast-ion velocity distribution.

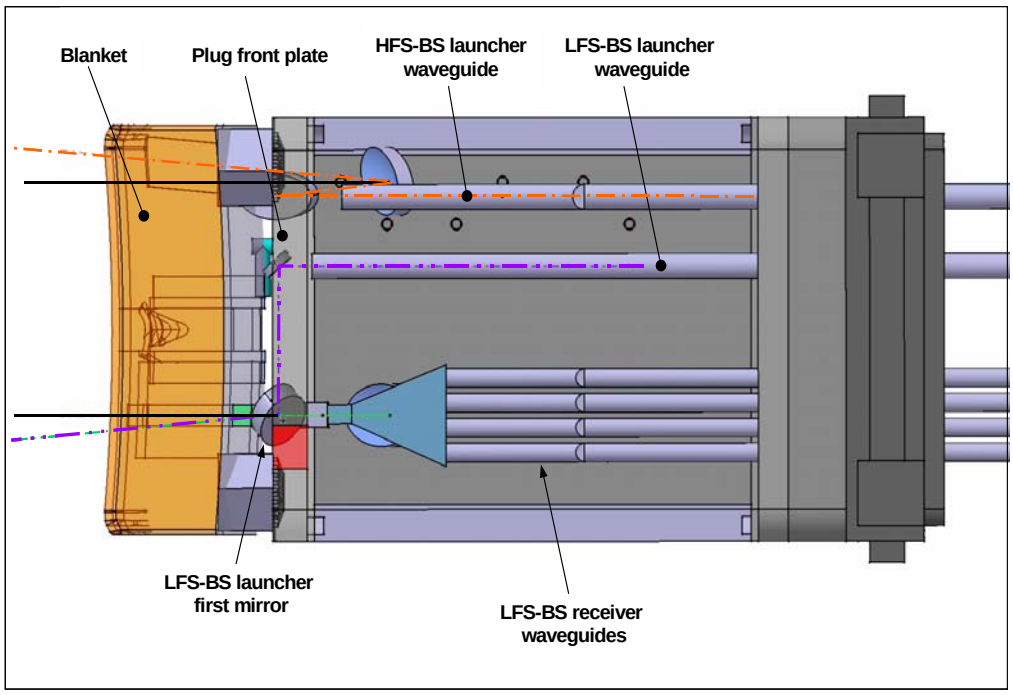

Figure 20. Top view of the CTS system in the port plug #12.

Each probe wave guide will have a CVD diamond window located just outside the plug back plate providing the primary vacuum boundary. As with the port plug components, these windows are water-cooled from the vacuum vessel primary heat transfer system.

The transmission lines in the port inter-space are straight and will contain support structures and expansion sections (expansion joints and elastic sections) to compensate vessel movements and thermal expansion. The second CVD diamond window is located just outside the bioshield providing the second vacuum boundary. After the CVD diamond widow, the waveguides are routed upwards by mitre bends and directed over the port cell door to the gallery. A waveguide flange just outside the bioshield and at the top of the bend will facilitate disassembling of the transmission lines when accessing the port plug. The transmission lines after the boishield (after the second vacuum boundary) will be evacuated and will have the standard safety components such as isolation valves, rupture disks sections, and DC breaks. Other components of the transmission lines include pumping sections, cooling systems, releasers, arc detectors, directional couplers, and movement compensation units.

As with the ECH&CD system, each line will have an RF conditioning unit to eliminate spurious modes, to select polarization and to shape the beam. The units also serve to switch in a dummy load needed for testing and conditioning of the gyrotrons.

Shown in Figure 21 is the layout of the CTS probe transmission line. For clarity, the transmission lines for the ECH&CD system are not shown. The waveguides for the CTS launcher follow the same route as the ECH&CD system from the RF building to the

gallery where a space of 500 mm spacing between waveguides is required. The path lengths from the heating hall to the tokamak building are about 20 to 30 m from the heating hall to the tokamak building and about 34 m from the south wall to the bioshield.

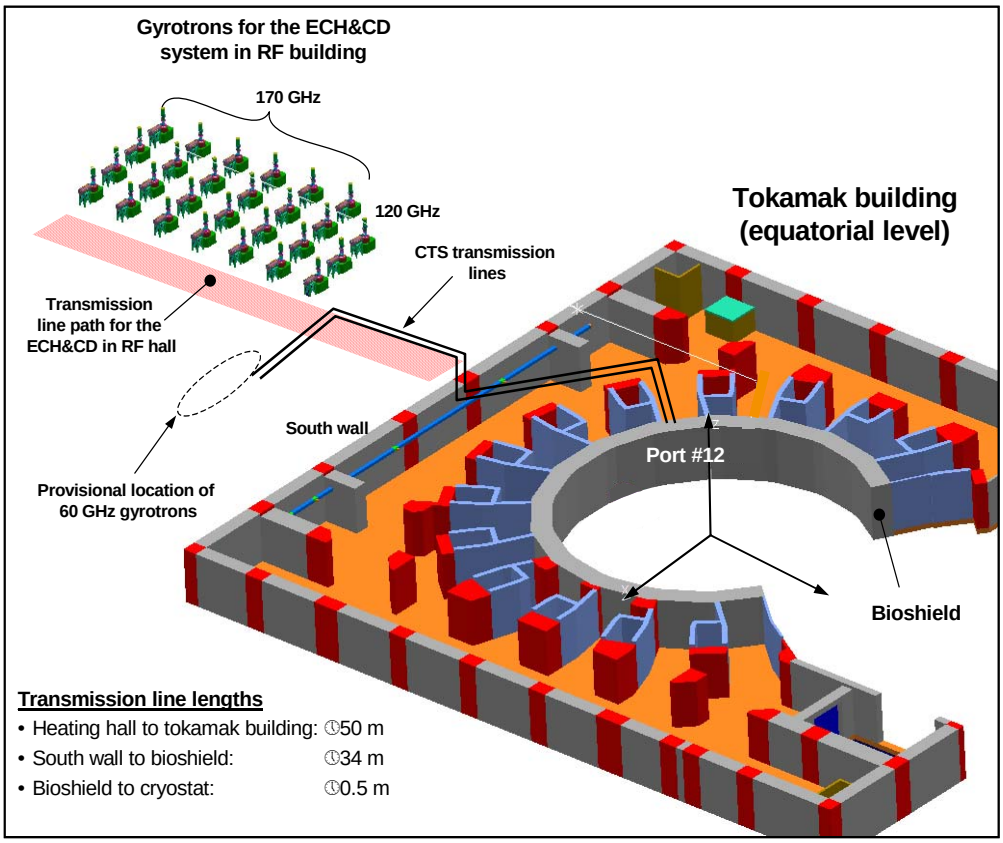

Figure 21. Layout of the CTS probe transmission lines from the gyrotrons hall to equatorial port #12. Shown in the figure are only the gyrotrons for the ECH&CD system. The path from the gyrotrons hall to the gallery will be the same as for the transmission line for the ECH&CD system (not shown for clarity).

4.1.3 RF source

The RF for the CTS probe at 60 GHz is generated by a gyrotron delivering RF power of 1 MW in steady state. Figure 21 shows the layout of the ECH&CD gyrotrons units that are located at the mezzanine level in the RF building. A minimum distance of 4 m between gyrotrons is required to avoid magnetic interference between gyrotrons. The 170 GHz ECH&CD gyrotrons are arranged in groups of 4 and the three 120 GHz gyrotrons are located as shown in Figure 21. The space available for the two CTS 60 GHz gyrotrons is indicated on the figure. The building design of the RF hall is still not complete; hence the allocated space for the CTS gyrotrons is still provisional. Each source will require its own RF conditioning unit. The RF test-stand and rig will be supplied from ECH infrastructure and has not been included as part of the CTS system.

4.1.4 Power supply

Power supplies, series switches, and other auxiliary support equipment are located immediately below each gyrotron on the lower level of the RF building. One key issue that needs to be addressed in the next design phase is the availability of space for the power supplies for the CTS gyrotrons. Presently, the design of the RF building does not have extra space for electric power sources for the two extra CTS gyrotrons on the ground level. This is due to the space reserved for an upgrade to additional ECH power.

4.2 LFS-BS receiver

The LFS-BS system is sub-divided in the following sections:

- In-vessel quasi-optical antenna system and waveguides.
- In-vessel calibration source
- In-vessel shutter / mirror mechanism
- Transmission line
- Diagnostic Hall signal distribution system and electronics

Another view from the plasma of the CTS system in the port #12 is shown in Figure 22.

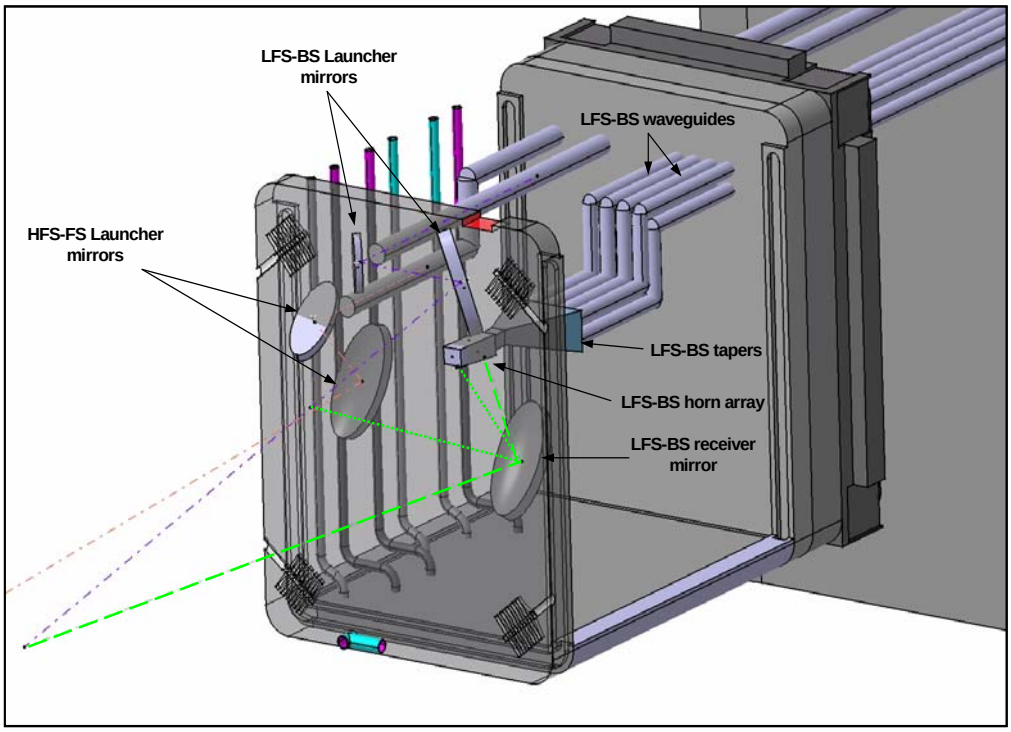

Figure 22. View of the CTS in port plug from the plasma side. The blanket is not shown and the plug front plate is semi-transparent.

The main components in each section are listed in the table in Appendix A.2

4.2.1 Front-end quasi optics

The dashed and dotted green lines in Figure 22 are the lines of sight of the receiver. The lines represent the upper and lower limits of the angular range in the viewing directions intercepting the line of sight of the LFS-BS system probe shown as the violet line. The LFS-BS receiver consists of an ellipsoidal quasi-optical mirror that couples radiation to a horn array distributed poloidally. Each horn is at a different distance from the first mirror in order that each viewing direction has its vertical beam waist in the plasma at the intersection with the probe. Figure 23 shows a closer view of the first mirror and the horn array, now viewed in the direction of the plasma. The enclosure shown in blue contains the fundamental waveguides that are directed to tapers and are couple to the overmoded waveguides.

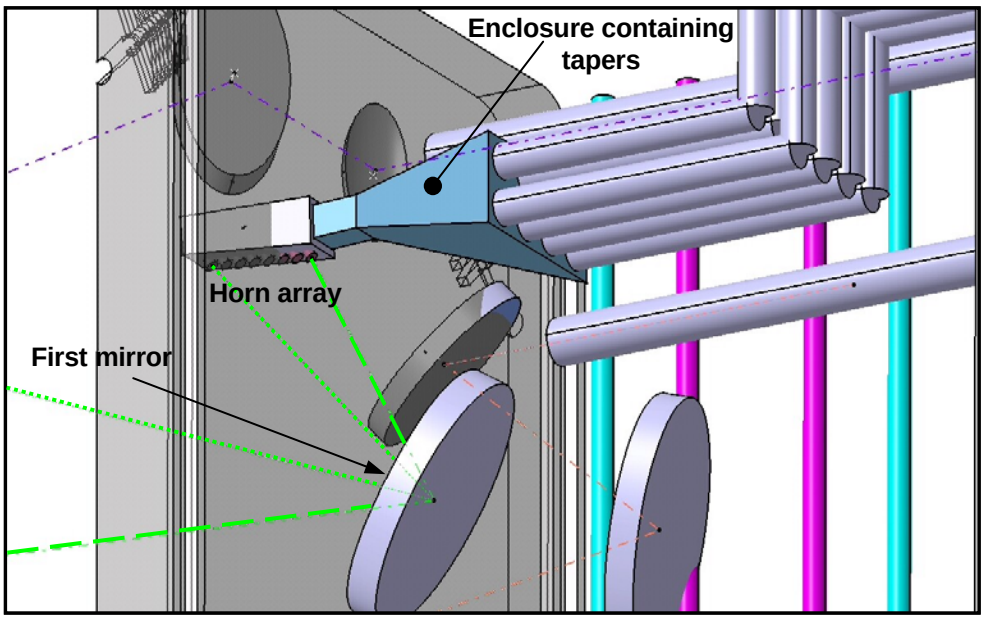

Figure 23. Closer view toward the plasma of the LSF-BS receiver first mirror and horn array.

The first mirror is located about 1.0 to 1.2 meters from the blanket's plasma facing surface. The dimensions of the mirror should be at least 300 H × 450 V mm. The material used for the first mirror is stainless steel. The horn array will also be made of stainless steel and be located just behind the blanket module.

Not shown in the design, is the calibration source and shutter mechanism that will be incorporated during the next phase of the design. The design of the calibration system will be based on the ECE system [5]. The calibration system consists of a calibration source and a shutter system directing radiation from the source to the first mirror. The shutter system will be the only moveable part of the CTS diagnostic.

4.2.2 Transmission lines

The transmission lines are made up of horns connected to fundamental waveguides coupled to overmoded waveguides. Only 8 waveguides are shown at present. The waveguides will direct scattered radiation from different locations in the plasma simultaneously. The cross sections of the overmoded waveguides can be expected to be no more than 20 mm.

The waveguides in the port are made of stainless steel. The waveguides will each have a window located just outside plug back pate determining the first vacuum boundary. Electrical breaks for the waveguides are incorporated on both sides of the window structure. Each waveguide will also have its own movement compensation unit immediately after the window in the inter-port space region. After the bioshield is a window forming the second vacuum boundary. An isolator valve is located after the window for easy isolation of the transmission line vacuum during removal. The waveguides are then directed upwards via mitre bends and are directed toward the gallery above the port cell doors. The waveguides from the bioshield are made of aluminium. There are 10 waveguides that run from the port cell to the diagnostic hall.

The total transmission loss due to this oxygen absorption at 1 atmosphere is negligible compared to the loss at the receiver electronics. However the absorption curve has a sharp peak at around 60 GHz with FWHM of about 10 GHz. This will significantly affect the calibration errors, hence evacuating or flushing the waveguides with a dry gas is needed.

4.3 HFS-FS receiver

The HFS-FS system is subdivided in the following components:

- In-vessel quasi-optical antenna mounted on inner vessel wall
- In-vessel transmission system to upper port plug
- Transmission line from port plug to port cell
- Transmission line to diagnostic hall
- Diagnostic Hall signal distribution system and electronics

The main components for the HFS-FS receiver are listed in the table in Appendix A.3

4.3.1 Front-end quasi-optics

The front-end quasi-optics for the HFS-FS system are located on the inner vacuum vessel wall. The design is shown in
Figure 24 without the blanket modules where the components are viewed from the plasma, and in
Figure 25, without the vacuum vessel, where the view is directed toward the plasma. A quasi-optical elliptical mirror is mounted on the vacuum vessel wall viewing the plasma from the vertical gap between the blanket modules (see Figure 6(a)). The mirror is located between the cooling manifolds below the blanket module key. The size of the mirror is limited by the available space between the cooling manifolds and is 350 mm in width. The radiation is collected and coupled to an array of horns below it. The distance between the mirror and the horn array is limited by the earth strap mounting block. The vertical distance available is 303 mm. Preliminary studies have shown that a marginal modification of the back portion of blanket modules is needed to accommodate the mirror. The mirror will be cooled by the vacuum vessel wall through conduction. Each horn collects scattered radiation from a different location in the plasma. This radiation is transmitted upwards via fundamental wave guides. Two pairs of 5 waveguides are directed upward along the vessel wall, behind the mirror, connecting to tapers that are couple to overmoded waveguides.

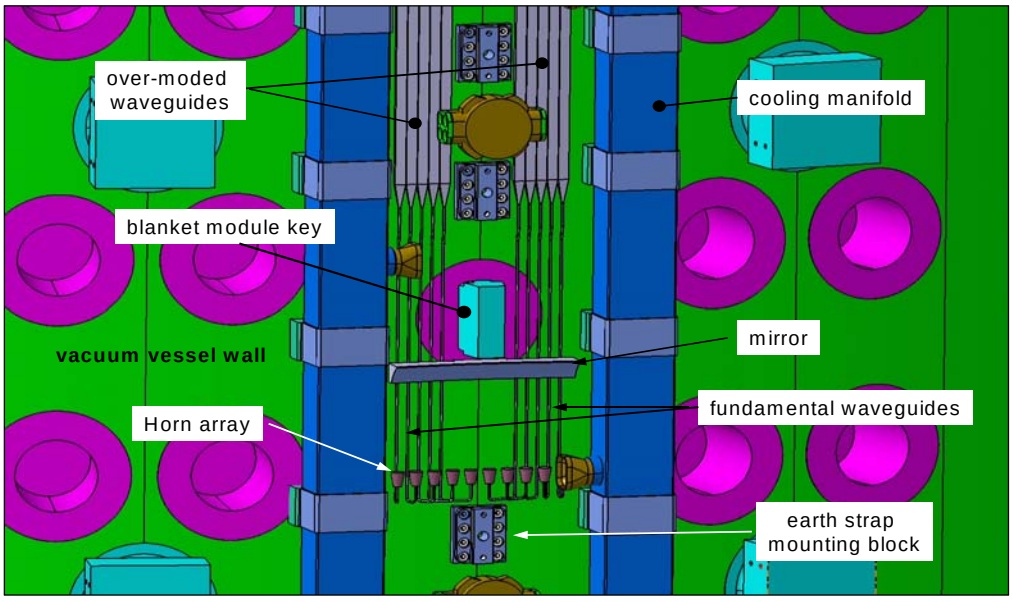

Figure 24. Design of the HFS-FS system viewed from the plasma. The blanket modules, earth straps, and the branch pipes connection the two manifolds are not shown.

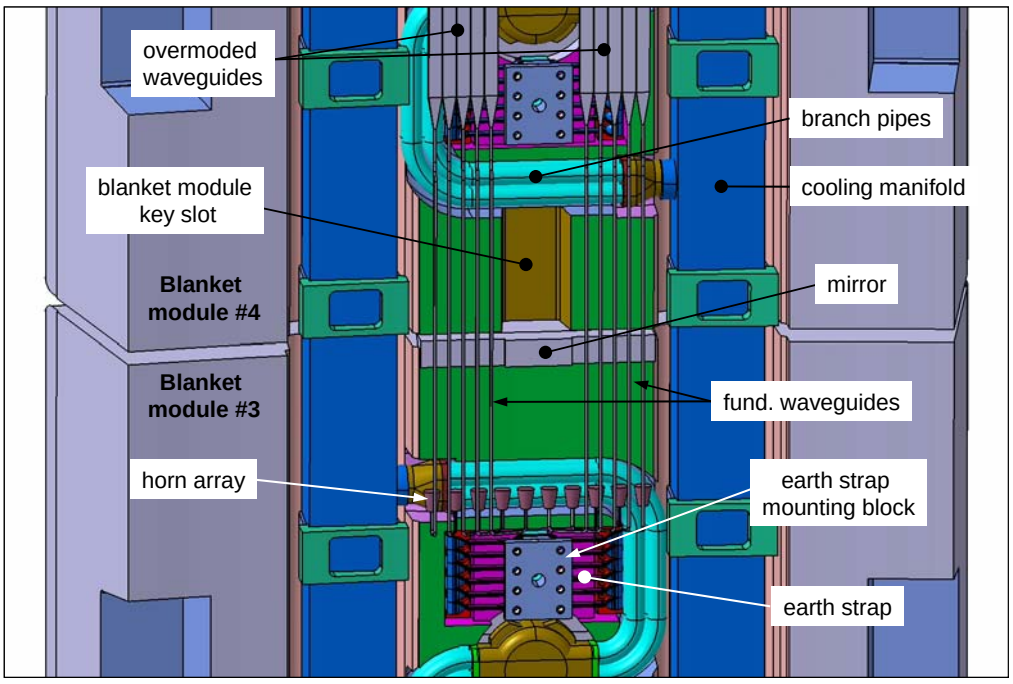

Figure 25. Design of the HFS-FS receiver system viewed from the inner vessel wall toward the plasma. Vacuum vessel wall is not shown

The mirror needs to be designed to maintain the quasi-optical qualities despite large neutron and heat flux. In addition, it must withstand disruption loads (eddy currents) and halo currents. The material to be considered to make a robust system can be stainless-steel, CFC, or tungsten.

4.3.2 Transmission lines

The in-vessel transmission line for the HFS-FS receiver consists or 2 pairs of 5 over-moded wave guides that are routed upwards along the vacuum vessel wall. The waveguides follows the same path as the in-board waveguides for the plasma position reflectometry diagnostic. The only difference in the path is that the CTS waveguides do not have the bend from the blanket gap. Therefore much of the design of the in-board wave guide system is based on studies presented in the Design Description Document of the plasma position reflectometry diagnostic [2]. The poloidal map of the waveguide path is shown in Figure 26. The figure shows four waveguide sections, *a* to *d*. The CTS HFS-FS receiver waveguides reside in a space behind the blanket modules reserved for wiring and diagnostics as shown in Figure 27. The toroidal width of this region is limited by the space between the contact points of the manifold and the earth strap mounting block. However, the toroidal width available throughout the path *a* to *d* is 104 mm toroidally by 32 mm radially and is illustrated by the blue-hatched regions of Figure 27. This width is limited at two key regions; the manifold anchor point and the removable manifold filler.

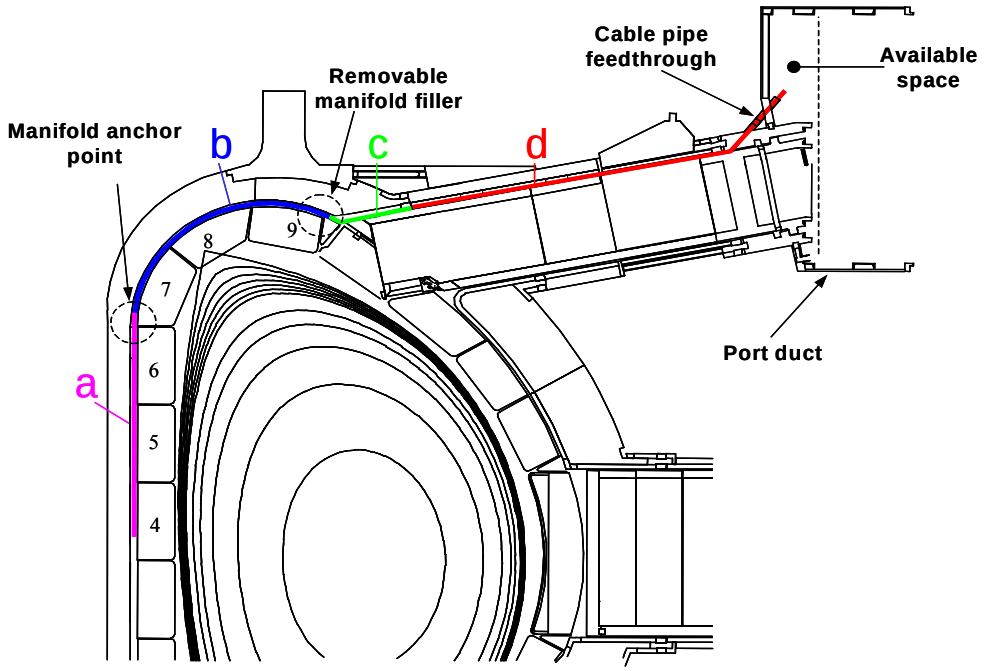

Figure 26. Poloidal map of the HFS-FS waveguide path along the vacuum vessel wall toward the upper port. Key regions where the available width is limited are encircled. Also shown is the path of the waveguide between the ceiling of the port and the port plug. The path follows through the provisional cable pipe feedthrough out into the port duct where the first vacuum boundary is located. The vertical dotted line indicates the radial position of the cast when accessing the port plug.

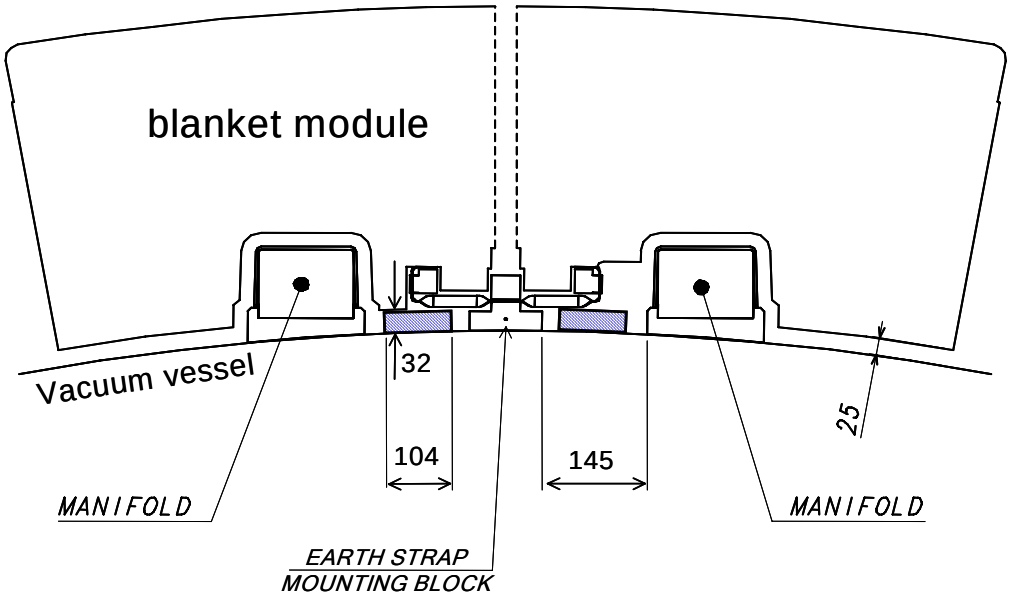

Figure 27. Top view of the blanket module on vacuum vessel. The blue hatched region is the clearance space throughout the path shown in Figure 26.

This region can accommodate 5 rectangular waveguides of 20×10 mm. Fundamental waveguides at 60 GHz frequency have dimensions of 3.8 ×1.9. The ohmic loss calculated for the fundamental waveguides and the over-moded ones are 1.56 and 0.065 dB/m respectively. Smaller over-moded waveguides with dimensions of 9×4 mm have Ohmic loss of 0.25 dB/m. These dimensions are sufficiently over-moded and the Ohmic losses can thus be neglected.

The waveguide path *a* is a straight 3 m long section. The waveguide paths *b* and *c* are shown in the 3-D drawing in Figure 28. This figure shows the in-board wave guides for the reflectometry diagnostic, the manifold, and the manifold filler. The view is from above the upper port looking downward towards the inner vessel wall. The only path available to the upper port is over the manifold filler shown in the figure. Since the path is not in the same poloidal plane as section *a*, the waveguide sections b and c deviate from the poloidal plane as they approache the manifold filler. Section *c* has two more bends in the long and short side. The waveguides in section *d* are parallel to the port and reside between the port plug and the ceiling of the upper port. The total size required by the conduit is expected to be less than 300×20 mm. Alternatives for bringing out the waveguides of vacuum vessel diagnostics have been considered. One possible solution is using the cable pipe at the top of the port as shown in Figure 26. Each of the upper ports has four provisional cable pipes for bringing out vacuum vessel diagnostic cables into the port duct. Waveguides can be brought through these pipes, with a possible change of pipe diameter to 80mm x 60mm [6]. The vertical dotted line in the port duct in Figure 26 is the radial limit of the cast when the upper port plug is being removed. Hence, the window assemblies are located in the region shown. This will eliminate disruption of the waveguides during port plug access. Therefore, the HFS-FS waveguides is not expected to affect the design of the ECH upper launcher.

The transmission lines from the inter-port space to the diagnostic hall are similar to the LFS-BS receiver transmission line described in Section 4.2.2. The only concern may be the available space in the inter-port region for the windows, DC breaks and movement compensation units. The waveguides are directed to the gallery in the upper level toward the diagnostic hall.

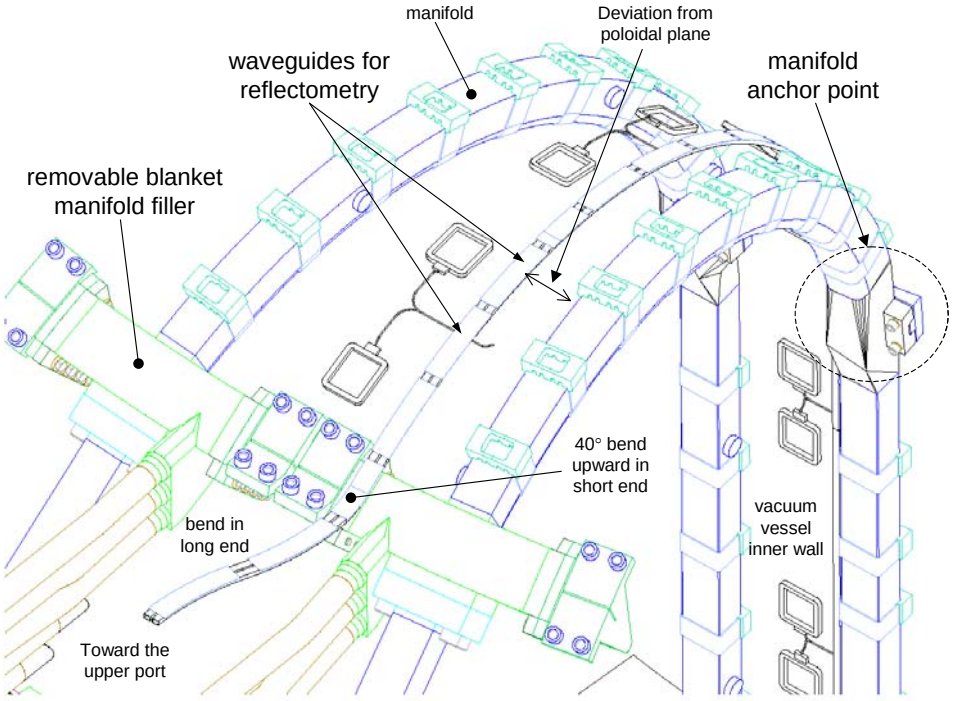

Figure 28. Design of the in-board reflectometry waveguides with the manifolds and manifold filler viewed from above and toward the inner side.

Attention needs to be given to the mode conversion caused by the bends in the waveguides. Three possible options should be studied further; gradual bends of varying sophistication as shown in Figure 28, mitre bends, and tapering down to fundamental or near fundamental. The Kurchatov group has shown promising results where a mock-up laboratory experiment carried out to analyze the performance of the in-board reflectometry waveguides with the bends in the ITER design [7]. The frequency used was 140 GHz with waveguide dimensions of 23×10 mm. Their experiments have shown

that the total power loss in the waveguide is of the same order of magnitude as the calculated resistive losses which are very small.

4.4 Acquisition system / receiver electronics

Each of the 10 receiver channels of the LFS-BS and of the HFS-FS systems will be equipped with heterodyne receivers. These will be composed as follows:

The CTS signal is transmitted in wave-guide into the EM-shielded environment where the rest of the receiver is located. Key parts include the notch filter, which attenuates stray radiation, the PIN switch, closed during switching of the gyrotron (modulated operation), which attenuates spurious gyrotron modes associated with switching transients, the down converter, which converts the CTS spectrum into a spectral range around 5-10 GHz, and the multiplexer which separates the sensitive wings of the CTS spectrum form the more robust central part. The wings are the principal carrier of information on the fast ions while the thermal bulk ion information is contained in the central part. After the multiplexer follows IF amplifier chains, succeeded by a filter bank, separating the signals into 50 separate band pass filters either by power dividers or by (frequency) multiplexers. After the band pass filters come detector diodes, followed by DC amplifiers and ADC's.

The spectral half-width of the fast ion feature, for the LFS-BS and HFS-FS system is between 2.4 - 4.5 and 0.5 - 1.5 GHz respectively, depending on the scattering angle and hence the radial location of the scattering volume. The narrowest full spectral width will thus be around 1.0 GHz, and locating 50 band pass filters within this range, corresponds to a filter width of 20 MHz. Such filters as well as the other parts of the receivers can be obtained with existing technology.

The ADC's currently in use for the TEXTOR and ASDEX Upgrade CTS systems have sampling rates of 100 k samples per second, which is adequate for the ITER CTS system.

5 Upgrade for measurement of fuel ion ratio

With an upgrade the LFS-BS system of CTS has the potential to provide temporally and spatially resolved measurements of the fuel ion ratio. Recall from Figure 20 that LFS-BS receiver and probe are oriented at an angle of about 5° from a poloidal plane. This is to avoid having the resolved fluctuation wave vector perpendicular to the magnetic field that will result in the fast-magnetosonic wave entering the spectrum, thus making it impossible to extract fast-ion information. However, measurements of the bulk ion feature with the resolved fluctuation wave vector perpendicular to the magnetic field has information which can be used to infer the fuel ion ratio. To achieve this, the system needs to be oriented in the near radial direction. This capability can be integrated into the CTS diagnostic requiring no additional openings in the plasma facing components and using the same first mirrors of receiver and probe. The upgrades mentioned below are the simplest and most robust method to upgrade the hardware to have a combined fast ion and a fuel ion ratio CTS diagnostic.

Probe upgrade. The upgrade includes: Larger second mirror, extra high power transmission line, and route switch in gallery.
Figure 29 shows the upgrade needed in to the LFS-BS launcher. The second mirror is modified to accommodate an extra beam emitted by the waveguide shown in red. The yellow dashed line shows the centre line of the probe beam to measure the fuel ion ratio. The launch direction is nearly in a poloidal plane. The two systems will use the same first mirror and RF source. Hence a route switch in the gallery, similar to the ECH&CD system, is required to redirect RF power to either system.

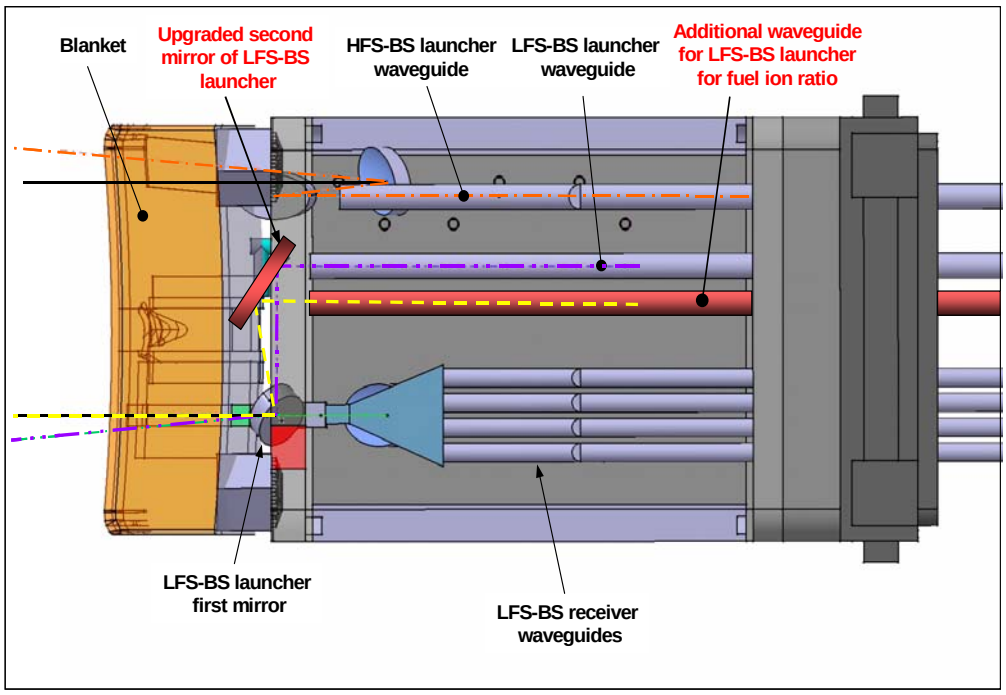

Figure 29. Top view of the CTS diagnostic in the equatorial port with the upgrade to the LFS-BS probe, shown in red, for measurement of the fuel ion ratio.

LFS-BS receiver upgrade. The upgrades include: Extra horn array, 2nd set of transmission lines, homodyne receivers with fine resolution over the bulk ion feature and acquisition. Figure 23 shows the horn array for the LFS-BS system. The horn array at not positioned in the same ploloidal plane as the first mirror resulting in an off-poloidal view. To view the plasma in directions near a poloidal plane, a second row of horns are located in nearly the same poloidal plane as the first mirror. Therefore a new set of transmission lines is needed. Estimating the fuel ion ratio relies on resolving the ion cyclotron harmonics in the bulk ion feature, which appear when the resolved fluctuations have wave vectors near perpendicular to the magnetic field. The fundamental harmonic frequency for an ion is $15.3 \times Z/\mu$ MHz / Tesla where Z is charge and μ is the proton mass ratio. Hence, the fundamental resonance for Deuterium and Tritium at B = 5.3 T is 40.5 and 27 MHz respectively. Therefore the frequency bandwidth needed to include at least 10 harmonics is of the order of 500 MHz. Hence, a homodyne receiver with 10 filter banks each sampled at 100 Msamples/s can be used.

Switching between the LFS-BS fast ion measurements and the fuel ion ratio measurements requires operation of a wave guide switch to redirect the probe. This can be done in a few seconds, permitting multiple switching between the two types of measurements in one plasma pulse.

6 Conclusion and future work

The integration of the 60 GHz CTS system can be integrated into ITER with existing and near term technologies. The system was design to satisfy ITER's measurement requirements for fast ions. The design is robust technologically and has no moveable components near the plasma. It provides measurements at different radial locations simultaneously. The CTS 60 GHz system has many components similar to other microwave diagnostics and the ECRH system. Therefore, many design studies can be done in parallel for these systems. Some modifications to the ITER components need to be done to accommodate the CTS. The most significant one is the 30 mm vertical gap

required between the HFS blanket modules where the HFS-FS system is measuring. There are no integration issues with other diagnostics yet identified in port #12. An upgrade to the LFS-BS system of CTS has the potential to provide temporally and spatially resolved measurements of the fuel ion ratio. The upgrade includes an extra high power transmission line with a wave guide switch, and an extra set of receiver horns and waveguides (10 each), and a relatively low cost receiver system.

There are technological issues needing attention for the CTS that are generic to microwave technology and will not be given detailed mention here. Research and development in areas such as materials, waveguide features, cooling etc. are common to the ECH&CD system and to other microwave diagnostics.

The technical issues that need further R&D that are particular to the CTS are as follows:

1) Development of a high power long pulsed source at 60 GHz. Long pulsed high power gyrotrons already exist for more difficult higher frequencies such as 140 GHz. The technologies have been tested successfully on current machines.

2) Due to the vessel movements, there will be misalignments of the receiver transmission lines. Experiments need to be done to determine the changes in calibration due to these misalignments.

3) Final design of the front-end quasi-optical components for the HFS-FS and LFS-FS system. This will determine the final sizes and shapes of all the mirrors. Performance of the front-end optics and transmission line need to be tested with full-scale laboratory mock-ups.

4) Method for calibration of the HFS-FS system.

5) One issue of concern is related to the fact that the CTS system is located in a remote handling port. Hence questions on the technological robustness of this microwave system against frequent dismantling of the transmission line in the interport space need to be studied in detail. Particularly the issues of alignment and conditioning of the high power transmission lines and effects on the receiver waveguides.

6) The importance of the antenna pattern form the HFS-BS receiver mirror is highlighted in Section 3.2. Mock-up experiments should be performed in order to verify the radiation pattern from the blanket gap.

7) Detailed design issues need to be studied regarding the space needed to accommodate the window assemblies for the large number of waveguides in the upper and equatorial port.

8) Optimisation of the type of waveguide and the size for the LFS-BS and HFS-FS receivers need to be studied.

A Component list

A.1 Probes

Port plug	**Number of units**
Front-end mirrors 1st mirrors ≈ 300 H × 400 V mm 2nd mirrors yet to be determined	4
Stainless-steel corrugated waveguides ≈60 mm diameter	2
Mitre bends	4
Port Inter-space	
CVD Diamond window	2
Stainless steel wave guides ≈60 mm diameter	2
Thermal expansion sections (bellows)	2
Port Cell	
Aluminum corrugated waveguides ≈60 mm diameter	2
CVD Diamond window	2
Mitre bends	4
DC breaks	4
Isolation valve	2
Vacuum pumping section	2
Gate valve	2
Support structures	6
Rupture disk section (or releaser)	2
Directional couplers/power monitors	2
Gallery	
Aluminum corrugated waveguides ≈60 mm diameter	2
Mitre bends	6
Directional couplers/power monitors	2
RF Conditioning unit	2
RF gallery	
Gyrotron units (Gyrotron tube, CVD diam. Window, magnet)	2
Aluminum corrugated waveguides ≈60 mm diameter	2
RF and DC electronics	2
Transformers and HV monitors	2
RF conditioning unit	2

A.2 LFS-BS Receiver

Port plug	**Number of units**
Front-end mirror (300 H × 450 V mm)	1
Horns and fundamental waveguides	10
Calibration system	1
Stainless steel waveguides (≈20 mm) (shape yet to be determined)	10
Mitre bends	20
Port Inter-space	
Stainless steel wave guides (≈20 mm) (shape yet to be determined)	10
Mechanical shutter transmission calibration	1
Fused silica window	10
Thermal expansion sections and bellows	10
Port Cell	
Aluminum waveguides ≈20 mm (shape yet to be determined)	10
SiN window	10
Mitre bends	20
DC breaks	20
Isolation valve	10
Gate valve	10
Gallery	
Aluminum waveguides ≈20 mm (shape yet to be determined)	10
Mitre bends	20
Rough vacuum pumping station	5
Burst disk assemblies	10
Isolator valve	10

A.3 HFS-FS Receiver

In-vessel	**Number of units**
Front-end mirror (350 H × 100 V mm)	1
Horns and fundamental waveguides	10
Stainless steel waveguides (20 × 10 mm)	10
Mitre bends	20
Port Inter-space	
Stainless steel wave guides (20 × 10 mm)	10
Fused silica window	10
Window assemblies	10
Thermal expansion sections and bellows	10
Port Cell	
Aluminum waveguides (20 × 10 mm)	10
SiN window	10
Mitre bends	20
DC breaks	20
Isolation valve	10
Gate valve	10
Gallery	
Aluminum waveguides (20 × 10 mm)	10
Mitre bends	20
Rough vacuum pumping station	5
Burst disk assemblies	10
Isolator valve	10

A.4 Acquisition system (LFS-BS and HFS-FS receivers)

	Number of units
EM-shielded cabinets and boxes	10
Filter bank (50 channels)	20
Detector front end	20
ADCs (50 channels)	20
Computer with software licenses	4

A.5 Fuel ion ratio (upgrade)

All dimensions are yet to be determined but are expected to be similar to the CTS system.

Probe upgrade

Port plug	**Number of units**
Larger 2nd mirror (size yet to be determined)	1
Stainless Steel Corrugated waveguide ≈60 mm diameter	1
Mitre bends	2
Port Inter-space	
CVD Diamond window	1
Stainless steel wave guides ≈60 mm diameter	1
Thermal expansion sections (bellows)	1
Port Cell	
Aluminum corrugated waveguides ≈60 mm diameter	1
CVD Diamond window	1
Mitre bends	2
DC breaks	2
Isolation valve	2
Vacuum pumping section	1
Gate valve	1
Support structures	3
Rupture disk section (or releaser)	1
Directional couplers/power monitors	1
Gallery	
Aluminum corrugated waveguides ≈60 mm diameter	1
Mitre bends	2
Directional couplers/power monitors	1
Route switch	1

Receiver upgrade (All dimensions are the same for the LFS-BS receiver).

Port plug	**Number of units**
Horns and fundamental waveguides	10
Stainless steel overmoded waveguides	10
Mitre bends	20
Port Inter-space	
Stainless steel wave guides	10
Fused silica window	10
Thermal expansion sections and bellows	10
Port Cell	
Aluminum corrugated waveguides	10
SiN window	10
Mitre bends	20
DC breaks	20
Isolation valve	10
Gate valve	10
Gallery	
Aluminum corrugated waveguides	10
Mitre bends	20
Rough vacuum pumping station	5
Burst disk assemblies	10
Isolator valve	10

Acquisition system upgrade

Acquisition system	**Number of units**
EM-shielded cabinets and boxes	3
Filter bank (10 channels)	10
Detector front end	10
ADCs (10 channels)	10

B References

1. H. Bindslev, F. Meo, S. Korsholm, ITER Fast Ion Collective Thomson Scattering, Feasibility study

2. ITER Design Description Document - Reflectometry For the Main Plasma (WBS 5.5.F.02)

3. ITER Design Description Document - Electron Cyclotron Heating and Current Drive System (DDD 5.2)

4. R.A. Olstad, J.L. Doane, C.P. Moeller, Y.A. Gorelov, H.J. Grunloh and M. DiMartino, Proceeding of the IAEA Technical Meeting on ECRH Physics and Technology for ITER, July 14-16, 2003, Kloster Seeon, Germany

5. ITER Design Description Document – Microwave Diagnostics (DDD 5.5.F)

6. C.I. Walker, Report # G 55 MD 166 03-11-04 W 0.1

7. V. A. Vershkov, S. V. Soldatov, D. A. Shelukhin, A. O. Urazbaev, V. G. Petrov, A. A. Petrov, Presentation given at the RF Progress Meeting on ITER/BPX Relevant Diagnostic Developments , St. Petersburg, Russia, July 15 - 16, 2003

Acknowledgments

We would like to thank the ITER and EFDA staff for their useful help and comments particularly, Chris Walker, George Vayakis, David Campbell, Damian Lockley, and Akira Sakasai. We also would like to thank Walter Kasparek and Dietmar Wagner for useful discussions.

Risø's research is aimed at solving concrete problems in the society.

Research targets are set through continuous dialogue with business, the political system and researchers.

The effects of our research are sustainable energy supply and new technology for the health sector.